Performance of a post-Byzantine Triple-domed Basilica under Near and Far Fault Seismic Loads:

Analysis and Intervention

Constantine C. Spyrakos, Charilaos A. Maniatakis, Panagiotis Kiriakopoulos, Alessio Francioso, Ioannis M. Taflampas
National Technical University of Athens, Greece

ABSTRACT

In this Chapter a triple-domed basilica constructed at the end of the 19th century is selected as a case study to present a methodology for the selection of the appropriate intervention techniques in monumental structures. The methodology includes in-situ and laboratory testing, application of analytical methods, consideration of geotechnical parameters and regional seismicity. Seismic loads are estimated according to contemporary and older concepts for seismic design. Since the impact of near-fault phenomena on masonry structures has not been thoroughly studied, although considered as responsible for extensive structural damage during major seismic events, a procedure is presented in order to account for the special characteristics of strong ground motion, in the so-called near-fault region. The seismic performance of the structure before and after interventions, using traditional and new technology, is assessed by applying a validated finite element model. Also, the out-of-plane behavior of structural parts is evaluated through kinematic analysis of selective collapse mechanisms.

Keywords: Historic Masonry Structure, Near-fault Phenomena, In-situ and Laboratory Testing, Finite Element Method, Kinematic Analysis, Intervention Techniques

1. INTRODUCTION

During the last two decades there is an increased interest on the maintenance of cultural heritage structures including monuments and historic buildings (Tassios, 2010). The willingness to protect cultural heritage is not exclusively an invention of our times; however, from the perspective of structural engineers there is a number of contemporary parameters that affect their contribution towards this effort.

The most important parameters could be considered the evolution of computational methods, instrumentation for non-destructive evaluation and new materials. Complicated analyses that would demand a vast computational cost a decade ago, nowadays may easily be performed (Spyrakos, 1995; Spyrakos & Raftoyiannis, 1997). New and more accurate instrumentation has allowed the collection of data with less intrusive approaches; thus, allowing the justification to use more elaborate analytical methods and smaller safety factors. The availability of this technology allows for a more scientific and rational application of

rehabilitation techniques. Furthermore, new materials are available, including fiber reinforced composites, which may provide solutions in difficult retrofit and strengthening problems. The need to use these materials in monumental structures arises from the limitations that do not allow extended modification in the inertia and/or stiffness characteristics of the overall structure, which may be mandatory with standard retrofit methods. Also, composite materials when properly applied quarantine durability and strength. The production technology and our understanding on the methods of their application continuously grow (Oliveira & Lourenço, 2006; Credali & Ussia, 2011; Spyrakos et al. 2011; Spyrakos et al. 2013).

The process of the overall restoration of a monumental structure requires an understanding of its structural system and behavior; a knowledge that can be obtained from an accurate determination of the stress and deformation distribution of the initial structure and the structure after the intervention. Current technology allows the use of complex and detailed analysis based on a detailed model, as a rule a finite element model, of the structure. An additional parameter that complicates the rehabilitation procedure is that, unlike modern structures, interventions on monuments are subject to restrictions resulting from national standards and international regulations; thus, a retrofit scheme should be not only technically feasible but also acceptable according to such limitations.

The necessity to protect structures of cultural significance has emerged by the fact that many of them have been constructed with no seismic regulations. Their design has been based on the experience of architects and construction techniques following concepts for seismic design available at the time of construction. As many of them are located in earthquake prone areas, such as the Mediterranean basin, not only they are characterized by significant seismic risk but in many cases they have already suffered damage from seismic activity. This reality has led to the establishment of provisions for the seismic strengthening of monuments (Decreto Del Presidente del Consiglio dei Ministri, 2011; Consiglio Superiore dei Lavori Pubblici 2009; Earthquake Planning Protection Organization, 2011).

Additionally, new findings in Engineering Seismology that derived mainly after the great earthquakes in Northridge, USA 1994 and Kobe, Japan 1995 have enriched our knowledge on strong ground motion characteristics at small distances from active faults, in the so-called “near-fault area” (Somerville et al. 1997). These special characteristics, yet not sufficiently accounted for in several seismic regulations, should be definitely considered in design in order to reduce damages in the near fault area (Spyrakos et al. 2008; Spyrakos et al. 2015).

In the context of the research program: “Seismic Protection of Monuments and Historical Structures” (SEISMO), a thorough methodology for the structural assessment, the conservation and restoration of monuments and heritage structures is developed, considering the previously discussed parameters. Several aspects regarding the seismic response of monuments and historical structures are investigated and advances in technical and analytical capabilities are employed in order to detect existing damage, obtain a reliable estimation of the actual behavior and propose measures to overcome structural deficiencies.

In the present study a discussion is made on the issues, addressed briefly above, that affect the conservation of monumental structures through the analysis and retrofit procedure of a post-Byzantine triple-domed basilica located in the island of Lemnos, Greece. The methods used to

assess the initial condition of the structure and the mechanical characteristics of the materials are presented in detail. The analysis uses seismic loads according to Eurocode 8 (Comité Européen de Normalisation, 2005; Comité Européen de Normalisation, 2005b) and the first Greek Seismic Code of 1959, GC-59 (Royal Decree, 1959); in addition, two earthquake scenarios that account for near-fault effects are examined. The Greek Seismic Code of 1959 can be used in Greece in order to assess the seismic response and apply retrofit measures to existing structures that have been constructed prior to 1985 and have suffered earthquake damage (Greek Government Gazette, 2014). The study involves a detailed finite element model in order to analyze the structure as a whole, while the out-of-plane behavior of structural parts is investigated through a kinematic analysis with macro-elements. Retrofit measures are suggested and their effectiveness is assessed by comparing the performance of the structure before and after the interventions.

2. HISTORICAL INFORMATION AND ARCHITECTURAL PERSPECTIVES

The 19th century can be considered as the most important period for the modern architecture for all the islands in the eastern Aegean. In the island of Lemnos, the exact location of which is depicted in Figure 1, this architectural growth has been recorded even from the travelers of that period (Tourptsoglou-Stefanidou 1986). In Figure 1, the traces of the North Anatolian fault in the vicinity of Lemnos are depicted with dashed line.

The church of St. Demetrius, located in Lemnos, has been selected as a case study of a historic structure constructed without seismic regulations in a seismically active region. It is a post-Byzantine triple domed basilica with a timber roof constructed between the years 1892 to 1902 to replace an older church (Palamida-Efthymiadou, 2007). The plan view is nearly quadrangle with three polygonal apses on the eastern façade (Figure 2). The length and width of the church are 25 and 21 meters, respectively. The central aisle has a vaulted ceiling, where a 5.6 m high dome and a Π-shaped outer narthex are incorporated. The height up to the base of the dome is 12m. The narthex maintains the typological and morphological characteristics of early Christian basilicas. The masonry construction is mixed including rubble masonry and carved corner-stones. The masonry is coated with plaster at the exterior facade of the church, while inside it is partly covered with coating and partly with frescoes. The pillars are made entirely with bricks of Byzantine type with a wooden core, as was the common practice at that period.

In January 2000, the church has been declared as a historic monument from the Greek Ministry of Culture, that also specified a peripheral protection zone of 50 m around the structure.

The seismic vulnerability of churches has been addressed in the literature (e.g., Mele et al. 2003; Lourenço, 2005; Asteris, 2008; Asteris et al. 2014) and has been re-confirmed during significant recent earthquake events, such as the M=7.1 Christchurch earthquake in New Zealand in 2011 (Dizhur et al. 2011) and two earthquakes with magnitudes of M=6.0 and M=6.1 that occurred in Cephalonia a Greek island on January 26th and February 3rd of 2014, respectively, that provoked extensive damages to churches made of unreinforced masonry with different architectural and mechanical characteristics (GEER-EERI-ATC, 2014).

3. CONDITION ASSESSMENT

Visual inspection as well as a series of in-situ and laboratory tests has been conducted for condition assessment of the church. Main objectives of the testing program were the collection of information regarding the mechanical and chemical properties of the materials as well as the construction details.

3.1 Geotechnical investigation

At first a geotechnical study was performed in order to investigate the stratigraphy of the soil and the level of groundwater table at the Church of St. Demetrius, followed by a soil amplification study. The scope of the geotechnical study was to provide the soil parameters needed to estimate the bearing capacity of the soil, the expected subsidence, the modulus of subgrade reaction and the soil category according to the Eurocode 8 (Comité Européen de Normalisation, 2005). The study of the dynamic soil response aimed at calculating a design spectrum that accounted for the amplification of seismic excitation through the local soil strata (Comité Européen de Normalisation, 2005).

The results of SPT tests for a representative borehole are shown in Table 1. As shown in Figure 3(a), the following layers have been identified: layer I: Artificial embankments consisting of sand and gravel fragments; layer II: fully weathered sandstone with interference of clay layers characterized by medium plasticity; and layer III: moderate to highly weathered sandstone and fine-grained sandstone with interference of clay layers at various depths. Also, In Figure 3(b), the specific weight γ, the modulus of elasticity E_S, the coherence c, the undrained cohesion c_u, the internal friction angle φ and the shear wave velocity V_S are shown for the three different soil layers. Based on the geotechnical investigation the soil was classified as type B according to the Eurocode 8 (Comité Européen de Normalisation, 2005).

Three accelerograms from representative Greek seismic events were selected in order to evaluate soil amplification: (a) the 1986 Kalamata earthquake with magnitude M=6; (b) the 1981 Korinthos (Alkyonides) aftershock earthquake at the Corinthian gulf with magnitude M=6.4; and the Athens 1999 earthquake with magnitude M=5.9 recorded at the Sepolia station. All three accelerograms were scaled to a maximum ground acceleration of 0.24g in order to be compatible with the seismic zone according to Eurocode 8 (Comité Européen de Normalisation, 2005). The scaled accelerograms excited the base of the soil column and the amplified spectra were obtained at the soil surface, as depicted in Figure 3(b).

3.2 Visual Inspection

A preliminary assessment of the condition may be performed with visual inspection and surveying which are usually applied to record damage, i.e., cracking, peeling or other imperfections in the structure. Noticeable cracking, observed almost everywhere on the internal and external facades of the Church, was recorded in detail and classified according to its type and size. Four major cracks developed in two diametrically opposed positions were observed, one at each external facade. Traces of the cracks are visible at the roof of the church; thus, it may be considered that they extend through the total height of the Church. The trace of these cracks appears to continue internally up to the vaults of the mezzanine. This crack pattern was more intense at the western façade, a trace of which could be seen on

the roof. Furthermore, most of the cracks observed on the ground floor have a trace on the parapet of the mezzanine. In Figure 4 the location and the shape of the crack pattern is depicted in all views of the structure. It should also be noted that significant cracking was also recorded at the vaults and the pillars.

It was observed that several steel tie-rods were placed to the initial construction at a latter stage as a strengthening measure; an indication that the building exhibited structural problems from the early years of its life. These steel elements have caused further damage to the masonry because of corrosion, as shown in Figure 5(a). Tie-rods, generally placed at the base of all the semicircular arches, follow the geometry of the structure in two horizontal levels: the first one is placed 1.80 m above the floor of the mezzanine and the other is much higher at 8.50 m. The second level regards the tie-rods supporting the semi-cylindrical bearing surfaces of the dome.

The internal tie-rods are manufactured by steel blades with different dimensions while the external rods have square hollow sections with external dimensions 3 cm x 3 cm. Advanced signs of oxidation have been observed on the external tie-rods while the interior ones present a much better condition. However, they are not placed continuously in each aperture and they do not have adequate anchorage; thus, their contribution should not be considered under seismic excitations.

At the bottom surface of the cross-vaults there exist oxidized and partially detached steel plates, as shown in Figure 5(b). Furthermore, one of the pillars in front of the temple has been strengthened with a reinforced concrete jacket, implying some local failure. The existence of local retrofit measures supports the supposition that the church has experienced damage in the past.

3.3 Measurement of Mechanical and Chemical Properties of Masonry

In order to measure the compressive strength of the stones and the bricks, both laboratory and in-situ tests were performed. Application of Rebound Hammer tests (American Society for Testing and Material, 2008; Tassios, 1988) at selected positions, in conjunction with the laboratory tests provided the compressive strength of the stones (lime stones): f_{bc}=45.8 MPa. The ASTM C 805 standard (American Society for Testing and Material, 2008) that was followed to conduct the Rebound Hammer test, although intended for use in concrete materials, may be adopted for use in masonry (Tassios, 1988). This procedure provides a loose correlation of surface hardness with material strength, provided that certain conditions are met, including: flatness of the tested surface; proper selection of the curve that relates the rebound number of the hammer to the strength, etc. For this reason, the Hammer test procedure should be combined with other methods in order to evaluate masonry strength properties, as discussed in the following.

The normalized compressive strength of masonry units, i.e., the compressive strength converted to the air dried compressive strength of an equivalent 100 mm wide by 100 mm high masonry unit, is used for design purposes according to Eurocode 6 (Comité Européen de Normalisation, 2005c). In order to calculate experimentally this normalized compressive strength, a number of masonry units are extracted from the structure and specimens of proper

dimensions are cut and compressed to failure; thus, obtaining their compressive strength (Tomaževič, 1999). The mean value of strength is then multiplied by a proper shape factor to account for the actual dimensions of each unit, compared to the standard dimensions 100 mm x 100 mm, according to EN 772-1 (Comité Européen de Normalisation, 2011).

Mortar samples were taken from various positions and their composition was examined at the laboratory. Sampling locations were chosen to be representative of the macroscopic characteristics and conservation measures that were taken in the past. The characterization of mortar was based on the composition and the microstructure. The laboratory work focused on the following issues:

- nature of mortar (e.g., hydraulic, mixed, etc.)
- composition of binder
- type and gradation of the aggregates
- ratio of raw materials

The following techniques were applied for the characterization of the mortar, as shown in Figure 6: (i) optical microscopy, (ii) study of the gradation of the aggregates, and (iii) X-Ray Diffractometry (XRD). Following a natural separation method of mortar-stone the results of X-ray diffraction showed that the binder of the mortar consisted of elf lime, during the carbonation of which calcium carbonate was formed that was widely detected in all samples. Furthermore, a significant quantity of quartz was detected. Based on extensive experience on similar mortars, non tensile tests were performed, and the compressive strength of the mortar was estimated to be f_{mc}=1 MPa.

The fragments-test method may be used to evaluate the tensile strength of mortar. The method is included between the least destructive tests for masonry (Katsaragakis, 1987; Tassios et al. 1990). At selected positions local deposition of coatings and revealing of masonry is carried out taking samples of mortar with irregular shape. The mortar samples are encased in appropriate matrices and subjected to direct tension (Tassios et al. 1990).

3.4 Infrared Thermography

An infrared radiation source is placed on one side of the control element and the flow of infrared energy is recorded and analyzed (Titman, 2001). Any gaps or inconsistencies in the body of masonry disrupt the flow of radiation and can thus be detected. This method is mainly used to detect corrosion, internal cracks, gaps, increased porosity and changes in materials of masonry of layout. Results of the method of Infrared Thermography at selected locations may be seen in Figure 7. Application of the method revealed areas of humidity at the walls and confirmed testimonies and historic data about the absence of either partial or full closure of openings.

3.5 Endoscopy

The conclusions drawn from visual inspection were confirmed through an endoscopic investigation. This method allows a direct visual observation of the inner part of masonry revealing the general structural layout and detailing. Endoscopy allows for the observation of the inner part of a masonry element, through an existing perforation or a new one that is

performed to allow visual inspection. The endoscopic devices allow measurements of inaccessible locations using a mobile head and lenses that can estimate distances with accuracy based on the stereoscopic effect (Leucci et al. 2011).

Endoscopy was applied to a total of five positions in the walls of the Church, that is four locations at a height ranging from 0.50 m to 1.00 m above the ground level and a fifth location at the mezzanine. In addition a number of endoscopies were applied at selected positions in order to examine the construction system of the central pillars and the anchorage length of the tie-rods in the masonry walls. The total number and the exact locations of the endoscopic investigation were determined considering the following parameters; (i) difference in construction periods; (ii) wall thickness that may imply differences in structural layout; (iii) distribution of damage; (iv) placement of strengthening divices, i.e., connection of tie-rods to the masonry body.

It was found that the bearing walls are composed by three-leaf masonry. There is no uniformity in the layout since stones of different sizes have been used at several locations. The stones are generally not carved while bricks are used mainly for the construction of the central pillars. Between the outer leafs there is a filler layer that consists of small stones and mortar of poor quality. The limited and small gaps in the middle layer of the wall, revealed by endoscopy, are fully compatible with this construction method (three-leaf masonry construction). In Figure 8 the endoscopic testing at the external wall next to the southern main entrance in the west façade.

3.6 Ambient Vibration Measurements

All structures and geological formations undergo permanent oscillations. These oscillations are provoked by various environmental disturbances such as, wind, waves, micro-tremors from the Earth's crust, movement and vibrations from human activity. The oscillations, so-called ambient vibrations, have low-amplitude and are characterized by a wide range of frequencies; thus, they could excite many significant modes of structures allowing their measurement (Kanai & Tanaka, 1961).

The modes of vibration and the natural frequencies of the church were measured applying with ambient vibration testing. There were conducted eight measurements in total with direction either western-eastern (WE) or north-south (NS) as shown in Table 2. The positions included the center of the church beneath the dome on the ground floor and the roof of the mezzanine as shown in Figure 9. Appropriate software has been used to calculate the transfer functions and the Fourier spectra at different positions.

In Figure 10(a) the location of the instruments during the first measurement is shown. The first instrument (channel 1) was placed on the ground and the second instrument (channel 2) at the base of the central drum. The measurement was performed in the East-West direction. The transfer function between the two channels is shown in Figure 10(b).

4. SPECIAL CHARACTERISTICS OF THE STRONG GROUND MOTION IN THE NEAR-FAULT AREA

4.1 Near-Fault Strong Ground Motion Characteristics

The increased density of recording stations in the near fault areas has permitted the collection of near-fault ground motion recordings that present characteristics quite different from those of the usual far-field ground motions. These near-fault characteristics are mainly present in the form of large pulses in the ground velocity time history records at sites towards which the fault ruptures, a phenomenon called directivity. The directivity phenomenon, its characteristics and effects will be briefly presented and explained in the following.

Rupture generally progresses across a fault as a series of individual cracks or sub-events. Each crack produces a dislocation or slip which has a duration called the rise time and a slip velocity or slip rate amounting to 50-150 cm/sec. Each crack creates a velocity pulse with duration equal to the rise time and amplitude equal to the slip rate. These pulses travel along the fault with the velocity of shear waves. At the same time the rupture spreads towards a certain direction with a rupture velocity similar to that of the shear waves. In the rupture direction, rupture cracks and crack velocity pulses travel with the same velocity. Accordingly, in the rupture direction, a phenomenon similar to the Doppler phenomenon takes place. The generated pulses overlap and the waves arrive at a site in the direction of rupture as a large pulse of motion creating a shock wave effect that occurs at the beginning of the record. The phenomenon is called forward directivity and the pulse of the ground motion is typically characterized by large amplitude and short duration. At a site located near the epicenter, where rupture propagates away from the site, the arrival of the pulses is distributed in time. This condition, referred to as backward directivity, is characterized by motions with relatively long duration and low amplitude (Somerville et al. 1997).

Rupture directivity effects can be present both for strike slip and dip slip events (Stewart et al. 2001). Because of its polarization, the pulse of motion is predominant in the orientation perpendicular to the fault plane. The same phenomenon is present for a dip slip fault, where forward directivity conditions occur for sites located near the up-dip projection of the fault plane. In this case, also, the pulse of motion is oriented perpendicularly to the dip of the fault plane.

4.2 Simplified Representations of Near-Fault Recordings

Research has shown that simplified representations of the velocity pulse can capture the salient characteristics of the response of structures to near-fault ground motions. The simplified pulse representations of velocity time histories are defined by the number of equivalent half cycles, the period of each half cycle and the corresponding amplitudes (Mavroeidis & Papageorgiou, 2003; Mavroeidis et al. 2004).

The period and the amplitude of the velocity pulses scale logarithmically with the moment magnitude of an earthquake. Strong motion recordings of recent large earthquakes confirm that the period of the near fault rupture directivity pulse increases with magnitude (Mavroeidis & Papageorgiou, 2003; Somerville, 1998; Alavi & Krawinkler 2000; Baker 2007). The period of the near fault pulse is related to source parameters such as the rise time, which generally increases with magnitude. Characteristically, for a moment magnitude of M=6 the pulse period can be less that 1 sec, whereas for large magnitudes of about M=8 such a period can be over 5 sec. As a rule, it can be stated that the rise time during an earthquake can be considered as 50% of the pulse period (Mavroeidis & Papageorgiou, 2003).

The amplitude of the velocity pulse is significantly affected by magnitude, distance and site conditions. Generally, use of a linear relationship provides the logarithm of the velocity amplitude from the magnitude and the logarithm of distance from the fault plane. The range of velocity amplitudes varies according to magnitude and distance from 20 up to 300 cm/sec (Somerville, 1998; Alavi & Krawinkler 2000; Bray & Rodriguez-Marek, 2004). Also, the number of half-cycles range from 1 up to 3, with a usual number of 2 half cycles. The number of half cycles affects the spectral amplification, that is, as the number of cycles increases the spectral amplification increases as well (Spyrakos et al. 2008; Mavroeidis & Papageorgiou, 2003; Taflampas et al. 2008; Taflampas et al. 2009; Maniatakis & Spyrakos, 2012). It should be noted that the literature suggests considering the pulse period to be equal to the predominant period of the 5% damping velocity response spectrum (Krawinkler & Alavi, 1988).

4.3 Near-fault Spectral Characteristics

After the presentation of the main characteristics of the velocity pulses it is of interest to refer the effects of these pulses on the elastic and the inelastic response spectra. First in what regards the elastic response spectra, it is observed that the acceleration spectra are amplified in the period range near the period of the directivity pulses (Mavroeidis & Papageorgiou, 2003). The ratio between the fault normal and the fault parallel components of the ground motion demonstrates that this amplification is bell shaped with a central period close to that of the directivity pulse (Baker, 2008; Shahi & Baker, 2011). The mean amplification value is 3 regarding the corresponding values of the fault parallel component. Generally, the fault parallel component represents the type of records not affected by directivity pulses. Accordingly, the fault parallel component generates spectra with a similar shape to the usual spectra given by seismic regulations and attenuation relationships (Boore & Atkinson, 2008). Thus, fault parallel spectra are in most cases comparable with design code spectra. The same bell shaped amplification is present in the displacement spectra where it can be seen that the fault normal spectra present a substantial amplification greater than the one specified in design code spectra. Procedures that incorporate amplification of the standard response spectrum to account for near-fault phenomena are available in the literature and are recently incorporated in the Next Generation of Ground Motion Attenuation, NGA, Project (Shahi & Baker, 2011; Boore & Atkinson, 2008; Abrahamson & Silva, 2008; Campbell & Bozorgnia, 2008; Chiou & Youngs, 2008; Idriss, 2008; Peer Strong Motion Database).

It is of interest discuss herein certain effects that are not taken into account in all NGA developed models. Of special interest is the effect of the hanging wall and the footwall in dipping faults. The hanging wall is the part of the fault over the fault plane on which the epicenter is usually located. In what regards the effect of the hanging wall on the ground motion at a site, it can be stated that sites situated on the hanging wall are much more affected than sites laying on the footwall, although both kind of sites may be equidistant from the upper edge of the fault rupture. Furthermore, it should be mentioned that for a buried rupture where there is not a surfacial indication of the fault rupture, the effect at the ground motion at a site are much stronger. The only exception is at the region next to surface eruption of the fault rupture in case the rupture is not buried.

In this study, the simplest but quite efficient model given by Boore & Atkinson (2008) was used. The model accounts for the magnitude and the distance scaling. Also, the effect of the hanging wall is considered by using the Joyner-Boore distance as the shortest distance from the site to the horizontal projection of the fault rupture. If the site is projected horizontally, the Joyner-Boore distance is taken as zero, an assumption that is quite efficient taking into account the hanging wall phenomenon. Also, the model takes into account the effect of the inelastic response of the site deposit, that is, the effect of the changes of the shear modulus and the damping of the soil deposit. Finally, in this study the spectra obtained from the Boore & Atkinson (2008) relationships were amplified for near field effects according to the method presented by Shahi & Baker (2011).

Regarding the inelastic spectra it appears that for periods smaller that the characteristic pulse period, ductility is quite greater than the corresponding reduction factor. As the period is reduced the ductility reduction factor ratio is increased. For periods equal to or larger than the pulse period, the ratio is close to unity with ductilities equal to the reduction factors. Usually for large periods this increase is up to the half of the pulse period (Mavroeidis et al. 2004). Even though there is considerable literature on reinforced concrete and steel structures considering near-fault phenomena, the study of masonry structures under near-fault seismic excitations is scarce compared to their significance in seismic design (Spyrakos & Maniatakis, 2006; Spyrakos et al. 2013b).

5. ANALYSIS

The mechanical characteristics of the masonry were based on the testing procedures applied. The compressive strength fwc of masonry was calculated according to the following expression (Tassios & Chronopoulos, 1986):

$$f_{wc} = \frac{2}{3}\sqrt{f_{bc}} - a + \beta f_{mc} \quad (1)$$

where: f_{bc} is the compressive strength of the stones; f_{mc} is the compressive strength of the mortar; α is a reduction factor (for masonry made of natural stone α=1); β is a factor that accounts for the mortar contribution on the masonry strength (for stone masonry β=0.5).

The tensile strength and the modulus of elasticity were obtained from the masonry compressive strength according to the following expressions:

$$f_t = f_c/10 \quad (2)$$

$$E = 1000 f_c \quad (3)$$

In Table 3 the mechanical properties of stone, mortar and masonry are presented for the initial state of the structure and the structure after interventions, which will be discussed in the following.

Two analyses were performed. Global analysis considers the structure as a continuum where all the inter-connected individual parts act and deform together during excitations. On the other hand local analysis identifies parts of the structure that may deform almost

independently from the whole bearing body. These parts, also referred as macroelements, may be determined with acceptable reliability based on a survey of the damaged structure. For example for a church an independently deformable structural part may include a cracked façade, an apse or a bell tower. The selection and evaluation of different possible collapse mechanisms is an issue of critical importance in order to assess the behavior of the structure, (D'Ayala & Speranza, 2003) since the assumption of a global mechanism may be adopted only when failure local mechanisms are excluded (Lagomarsino et al. 2013; Pantazopoulou, 2013).

The macroelement approach may be usually followed by either a kinematic limit analysis or a non-linear static analysis. The first alternative, which has been selected in this article, involves the proper selection of a collapse mechanism, while the second one uses a finite element model as well as a "blocks and joints" analysis (Spyrakos et al. 2013; PCM 2014; Pugi, 2013).

5.1 Static and Seismic Loads

The loads considered in the analyses include:

- **Dead loads:** the self weight of the structure that derives automatically from the geometrical characteristics of the individual parts and the mass density of each material.
- **Live loads:** it applies to a uniform load of 5.0 kN/m2 for C3 category of use that was considered at the mezzanine. The mezzanine is an area of crowd concentration; thus, according to the Part 1 of Eurocode 1 it may be assigned to the C3 category (Comité Européen de Normalisation, 2002).
- **Seismic loads.** The seismic loads were determined according to: (i) the current version of Eurocode 8 (Comité Européen de Normalisation, 2005; Comité Européen de Normalisation, 2005b); (ii) the first Greek Seismic Code adopted in 1959 (Royal Decree, 1959); (iii) spectra accounting for near-fault effects.

Greece is the most seismically active region in Europe and among the most seismically active regions on a global scale (Tsapanos & Burton, 1991). The island of Lemnos in the north Aegean Sea is located in a seismic zone II that is characterized by a reference peak ground acceleration a_{gR}=0.24 g according to the seismic zone map of Greece (Hellenic Organization for Standardization, 2009). The North Aegean is a well known area for its high seismicity with strong earthquakes reported even from ancient historical era up to as recently as 2014 (Papazachos & Papazachou, 2003): M=7.0 in 197 BC; M=7.0 in 1471; M=7.0 on May 14, 1887; and M=6.8 on August 6, 1983. Most recently on May 24, 2014, a M=6.3 earthquake occurred with an epicenter between the islands of Lemnos and Samothraki, as the result of strike-slip faulting at shallow depths beneath the northern Aegean Sea. Faults within the North Aegean trough represent the northern branch of the North Anatolian fault system, the major transform faulting structure in northern Turkey (USGS webpage).

In Figure 11 the different spectra applied in the analyses are shown. The Eurocode 8 spectra were considered with the following characteristics: reference ground acceleration for seismic zone II; a_{gR}=0.24 g; importance factor γ_I=1.2, characteristic periods T_B=0.15 sec, T_C=0.50 sec and T_D=2.00 sec and soil factor S=1.2. The near-fault spectra are determined applying the procedure proposed by Shahi & Baker (2011) and can be representative of an M=6.5 seismic

event, average shear velocity $V_{S,30}$=360 m/sec and distance from the surface projection of the fault R=1 km and R=5 km, denoted as NF-1 and NF-5, respectively. The elastic spectra are depicted with a continuous line, dotted lines correspond to inelastic spectra and dashed lines correspond to mean spectral acceleration ± one standard deviation for the NF-5 scenario. A behavior factor q=1.5 was considered for all cases indicating a structure with small ductility. This value of the behavior factor is suggested by the current Eurocode 8 for unreinforced masonry structures (Comité Européen de Normalisation, 2005). The results from spectral analysis for the NF-5 scenario are not presented in detail, since as shown in Figure 11, they correspond to spectral values lower than the EC8 spectrum for the range of periods considered; thus, it could provoke less damages than the EC8 spectra. However, this overall conclusion is valid in average sense only, since consideration of the mean spectrum plus one standard deviation (NF-5 + 1σ) might be more damaging even from the NF-1 scenario, as also depicted in Figure 11. For clarification, it is mentioned that R=1 km or R=5 km indicate epicenter distances that could be in the range of 15 to 25 km. These values are indicative and could be adopted on the basis of the vicinity of Lemnos with the traces of the North Anatolian fault, as shown in Figure 1.

5.2 Global Analyses and Results

The finite element model, shown in Figure 12, consists of 317929 six and eight-node solid elements. The tie-rods were modeled using linear finite elements with six degrees-of-freedom at each node.

Prior to the response spectrum analysis, an eigenvalue analysis of the model was performed and the results were validated based on the results of the ambient vibration testing. The first three modes of vibration without the contribution of tie-rods are shown in Figure 13.

Further the analytical results allowed the validation of the finite element model, since they predicted with considerable accuracy the location of major cracks observed from the surveying. A typical example of validation regarding the north façade is shown in Figure 14. The distribution of maximum stresses, for all the different spectra, are depicted in Figures 15, 16, 17 and 18 for the west, south, east and north façade, respectively. It should be noted that grey colors in the contour diagrams indicate exceedance of the tensile strength. The grey color denotes failures that occur nearly at all facades and for all cases regarding the initial structure prior to the interventions.

As depicted in Figure 11 the maximum demand is imposed from the near-fault spectrum at R=1 km, NS-1, while the second most damaging loading should be expected for the other spectrum in the near-fault area at R=5 km, NS-5. Indeed the maximum stresses for seismic combinations are noticed for the NS-1 spectrum, as shown in Figures 15-18 (c) while the NS-5 seismic scenario also results in extended damage as shown in Figures 15-18 (d). The eigenperiod at each direction and the corresponding spectral acceleration for each spectrum are shown in Table 4. Notice that the West-East direction was set as direction x-x. The capacity checks included:

- In plane flexural resistance
- Shear resistance
- Out of plane flexural resistance parallel to the joints

Figure 19 shows the pillars and lintels that fail according to the analysis. The rate of failure is assessed based on the ratio *a*=Demand/Capacity. A yellow color is selected to show slight avoidance of failure or slight exceedance of the capacity when $0.90 \leq \alpha \leq 1.1$. The red color depicts the elements with significant failure, i.e., $\alpha > 1.1$. Magenta denotes failure in tension.

5.3 Local Analyses and Results

The systematic inspection of the construction details, knowledge of the masonry typology, the presence of earthquake-resistant elements and the visual inspection of existing cracks and damages allowed to identify the structural macroelements and to foresee which collapse mechanism is more likely to develop for the St. Demetrius Church. The determination of possible collapse mechanisms allows for a study of the out-of-plane behavior through a kinematic limit analysis of these mechanisms. Given the pattern of the cracks existing on the structure, two collapse mechanisms are examined, that is, the overturning of a part of the left façade and the overturning of the central apse, as shown in Figure 20.

Through kinematic analysis one may calculate the collapse multiplier α0 using the principle of virtual work given in the following form (Consiglio Superiore dei Lavori Pubblici, 2009):

$$\alpha_0\left(\sum_{i=1}^{n} P_i\delta_{x,i} + \sum_{j=n+1}^{n+m} P_j\delta_{x,j}\right) - \sum_{i=1}^{n} P_i\delta_{y,i} + \sum_{h=1}^{o} F_h\delta_h = L_{fi} \quad (4)$$

where: $\boldsymbol{n}$ is the number of the weights applied to the different blocks of the kinematic system; $\boldsymbol{m}$ is the number of the weights non-directly applied to the blocks, which because of the seismic action transfer a horizontal force to the blocks; $\boldsymbol{o}$ is the number of the non-related to masses external forces applied to the blocks; $\boldsymbol{P_i}$ is the generic weight applied to the block (self-weight applied to the centroid or any other carried weight); $\boldsymbol{P_j}$ is the generic weight (non-directly applied to the blocks) which, because of the seismic action, transfers horizontal forces to the blocks; $\boldsymbol{\delta_{x,i}}$ is the virtual horizontal displacement of the $\boldsymbol{P_i}$ weight application point; $\boldsymbol{\delta_{y,i}}$ is the virtual vertical displacement of the $\boldsymbol{P_i}$ weight application point; $\boldsymbol{F_h}$ is the absolute value of generic external force applied to the blocks; $\boldsymbol{\delta_h}$ is the virtual displacement of the $\boldsymbol{F_h}$ force application point in its direction and $\boldsymbol{L_{fi}}$ is the work of internal forces. In equation (4) the x-x direction is the direction of the collapse of each mechanism that is normal to the direction of the axes of rotation in case of overturning.

The spectral acceleration $\boldsymbol{a_0^*}$ that causes the collapse mechanism is given by:

$$a_0^* = \frac{a_0 g}{e^* FC} \quad (5)$$

where $\boldsymbol{e}^*$ is the "participating mass ratio" calculated from the following equations:

$$e^* = \frac{g \cdot M^*}{\sum_{i=1}^{n+m} P_i} \quad (6)$$

$$M^* = \frac{\left(\sum_{i=1}^{n+m} P_i\delta_{x,i}\right)^2}{g\sum_{i=1}^{n+m} P_i\delta_{x,i}^2} \quad (7)$$

and *FC* is the confidence factor taken as equal to 1.35 for kinematic analysis.

The macroelement response fulfils the ultimate Limit State when

$$a_0^* \geq \mathrm{Max}(a_{Rig}^*, a_{Def}^*) \quad (8)$$

where $\boldsymbol{a^*_{Rig}}$ and $\boldsymbol{a^*_{Def}}$ are the accelerations that the structure should sustain assuming that the structure underneath is rigid or deformable, respectively. $\boldsymbol{a^*_{Rig}}$ and $\boldsymbol{a^*_{Def}}$ are given by the following expressions:

$$a^*_{Rig} = \frac{a_g\, S}{q} \quad (9)$$

$$a^*_{Def} = \frac{S_e(T_1)\, \Psi(Z)\, \gamma}{q} \quad (10)$$

where: $\boldsymbol{a_g = \gamma_I a_{gR}}$ is the ground acceleration, $\boldsymbol{S}$ is the soil factor and q is the behavior factor taken equal to 1.5, $\boldsymbol{S_e(T_1)}$ is the elastic spectrum calculated for the period $\boldsymbol{T_1}$ that is the first period of vibration of the structure in the considered direction; $\boldsymbol{\Psi(Z)}$ is the first mode of vibration in the considered direction normalized in order to be equal to 1 at the top of the structure, Z is the height of the rotation axis with respect to the building foundations and γ is the correspondent modal participation coefficient.

The use of the near-fault spectra affects the term $\boldsymbol{a^*_{Def}}$, since it refers to the factor $\boldsymbol{S_e(T_1)}$ of the elastic spectra. The terms $\boldsymbol{a^*_{Def(EC8)}}$ and $\boldsymbol{a^*_{Def(NF)}}$ are defined as the required accelerations for a deformable structure under the macroelement according to Eurocode 8 and the near-fault spectra, respectively.

Table 5 shows the results of the kinematic limit analysis performed for the two macroelements as well as the results of the verification with respect to Ultimate Limit State according to Eurocode 8 and the NF-1 and NF-5 near-fault spectra. The verification were performed with the spectra shown in Figure 11 considering an importance factor $\boldsymbol{\gamma_I = 1.2}$. This value of γ is suggested by Eurocode 8 for structures that belong to importance class III whose seismic resistance is significant for the preservation of cultural heritage (Comité Européen de Normalisation, 2005).

The verifications performed for the collapse mechanisms of the left façade and the central apse yielded different results depending on the spectra.

According to EC8 and NF-1, both macroelements do not reach the Ultimate Limit State, being

$$\boldsymbol{a^*_0 \leq Max(a^*_{Rig}, a^*_{Def})}$$

Instead the NF-5 verification shows that the collapse mechanism of the left façade fulfil the requirements in terms of the spectral acceleration being

$$\boldsymbol{a^*_0 \leq Max(a^*_{Rig}, a^*_{Def})}$$

while the macroelement of the central apse does not reach the ultimate state; however, the acceleration that activate the mechanisms is very close to the requirement, i.e.,

$$\boldsymbol{a^*_0 \cong a^*_{Rig}}$$

Red colour in Table 4 denotes collapse, while green colour denotes fulfillment of the Ultimate Limit State.

6. INTERVENTION SCHEME AND PERFORMANCE OF THE STRENGTHENED STRUCTURE

The assessment of the current condition of the structure revealed significant problems that may affect the structural behavior including extensive cracking of the masonry walls at all façades and mortar of poor quality. The existence of damage, nearly from the construction period, can be attributed to the limited strengthening measures that have been taken. Response spectrum analyses revealed that there is a number of significant exceedances in capacity at many positions. Failure is expected for seismic loads according to the current Eurocode 8, while more extensive damage should be expected for seismic loads corresponding to near-fault phenomena. Moreover the results of kinematic analyses imply an out-of-plane failure for a wall of the mezzanine at the north façade for the NF-5 spectra and an overturning of the central apse for both the EC-8 and the NF-5 spectra.

In order to overcome these structural weaknesses, a retrofit and strengthening scheme is suggested that includes the following measures:

1. Replacement of tie-rods with steel bars of a 20mm diameter.
2. Consolidation of the masonry through grout injections. The grouting will be carried out only through the outer façades of the walls at the first level of the Church.
3. Application of carbon fiber sheets (CFRP) at selected locations of the bearing structure to improve tensile strength or, as an alternative, use a stainless steel grid of a particular form and size.

The consolidation of three-leaf masonry walls may be accomplished applying injections with grouts of compressive strength in the range of 10 MPa (Oliveira & Lourenço, 2006; Spyrakos et al. 2013; Vintzileou & Miltiadou-Fezans 2008; Corradi et al. 2008). The compressive strength of the wall after injection, $f_{wc,s}$, may be determined for f_{gr} denoting the compressive strength of the injected material according to the relationship:

$$f_{wc,s} = f_{wc,0} + 0{,}31(V_{\inf} / V) f_{gr}^{1{,}18} \quad (11)$$

where $f_{wc,0}$ is the compressive strength prior to grout injection and V_{inf} /V is ratio of grout to masonry volume (Valluzzi et al. 2004). In Table 3 the mechanical properties of the materials for the strengthened bearing structure are presented.

The use of carbon fiber sheets impregnated with inorganic resins to upgrade mechanical properties of masonry has received increased application during the last decades (Oliveira & Lourenço 2006; Spyrakos, 2004; Spyrakos et al. 2012). The placement of CFRP sheets is reversible and does not change the aesthetics of the structure, after competition, since it involves the application of very thin layers placed between two layers of coating. The CFRP sheets were applied at the exterior surface of the roof and at selected positions of all façades as depicted in Figure 21. Two-plies of carbon fiber sheets, with carbon sheet thickness of 0.17 mm per ply, and 0.50 m width were selected. The mechanical properties of the carbon fiber

are: modulus of elasticity E_c=240 GPa and ultimate strength f_j=3500 MPa. The tiles of the roof are temporarily removed and replaced after the placement of CFRP sheets.

Carbon polymer reinforced strips are also placed at the bottom surface of cross-vaults to replace the existing steel plates, as shown in Figure 21(d). The CFRP strips combine high durability and fire resistance with significant strength.

The results of the modal analysis for the structure after the interventions are shown in Table 4, where a decrease of natural periods in both directions of the structure is observed. However, this alteration in the first mode slightly affects the corresponding spectral acceleration.

Modal response spectrum analysis is performed for the four seismic scenarios and the results regarding the structure after interventions are depicted in Figures 22, 23, 24 and 25 for the west, south, east and north façade, respectively. For reasons of comparison, Figures 22-25 follow the same arrangement with Figures 15-18 that correspond to the stress distribution in initial condition prior the interventions. After the application of the rehabilitation scheme the exceedance of tensile strength is limited mainly at masonry elements of decrease structural value, as regards the stress distribution for the EC-8 and the GC-59 spectra (Figures 22-25 (a) and (b)). The greater part of the façades surface is depicted with a pale color in the contour display that suggests non-exceedance of the tensile strength. Maximum displacement at the top of the dome is 13.7 mm, a value acceptable for life-safety performance.

The decrease of maximum stresses is also obvious for the NF-1 and NF-5 spectra. However, significant damage may be expected at significant parts of all façades, especially for the near-fault scenario NF-1, even for the strengthened structure as shown in Figures 22-25(c). Overcoming these structural weaknesses, although technically feasible, requires major architectural interventions that could alter the historical character of the monument.

7. CONCLUSIONS

This study presents a comprehensive methodology that combines in-situ and laboratory testing with structural modeling leading to the selection of the appropriate intervention measures on historic structures. It demonstrates the significance of near-fault effects and the need to be accounted for and, finally the use of both traditional and modern state-of-the art techniques for effective strengthening that respect the historic and architectural characteristics of the monument.

Emphasis is placed on the assessment of the adequacy of older and current seismic codes to account for near fault phenomena, an issue of great importance for areas of high seismicity, such as Greece. The declared historic monument triple-domed basilica was constructed at the end of the 19th century in Lemnos, Greece. The rhythm of construction, with typical post-Byzantine characteristics, suffers from significant deficiencies including extensive cracking on the masonry walls, poor quality of mortar and corrosion of steel elements. The assessment of the current condition of the monumental temple was made by the application of detailed surveying, in-situ and laboratory testing. The mechanical properties obtained by testing were used for the development of the finite element model and the dynamic properties of the structure were used in order to validate the finite element model.

The study of dynamic response included: (i) modal analysis; (ii) Modal Response Spectrum analysis with a global finite element model; (iii) kinematic analysis for the assessment of out of plane behavior involving possible collapse mechanisms. Four earthquake scenarios have been considered including seismic loads according to: (i) the current Eurocode 8 provisions; (ii) the first Greek Seismic Code, GC-59, enforced in 1959; (iii) near-fault seismic conditions for M=6.5, $V_{S,30}$=360 m/sec and distance from the fault R=1 km and R=5 km, denoted as NF-1 and NF-5, respectively.

In summary for the structure in its present condition, the global analysis confirmed that: (i) the cracking observed by visual inspection occurred at locations of maximum stress, (ii) excessive damage should be expected even for the seismic loads of GC-59, and (iii) the near-fault conditions emerged to be even more damaging with the NF-1 scenario being the worst. Local analyses showed that the central apse and the mezzanine wall at the north façade turn out-of-plane for both the EC-8 and the NF-1 spectra, while both mechanisms fulfill the Ultimate Limit State for the seismic loads according to the NF-5 scenario.

In order to confront the above structural deficiencies strengthening measures have been applied. Response spectrum analysis of the model after the interventions implied that the strengthened structure may undertake the seismic loads according to the GC-59 with only limited damage at secondary elements and the seismic loads according to EC8 with significantly less damage compared to its initial state prior to the interventions. It also showed that the overall response is drastically improved also for the near-fault scenarios; however, there exist parts of the structure where significant damage could occur. Protection of the structure for the near-fault conditions would require further interventions, a task that in many cases would require intrusive interventions.

REFERENCES

Abrahamson, N.A., & Silva, W. (2008). Summary of the Abrahamson&Silva NGA ground-motion relations. *Earthquake Spectra*, *24*(1), 67–97.

Alavi, B., & Krawinkler, H. (2000). Consideration of near-fault ground motion effects in seismic design. In *Proceedings of the 12th World Conference on Earthquake Engineering* (article 2665). Upper Hutt, N.Z.: New Zealand Society for Earthquake Engineering.

American Society for Testing and Material (ASTM). (2008). Standard C 805/C 805M – 08. Standard Test Method for Rebound Number of Hardened Concrete.

Asteris, P.G. (2008). On the Structural Analysis and Seismic Protection of Historical Masonry Structures. *The Open Construction and Building Technology Journal*, *2*, 124-133.

Asteris, P.G., Chronopoulos, M.P., Chrysostomou, C.Z., Varum, H., Plevris, V., Kyriakides, N., & Silva, V. (2014). Seismic vulnerability assessment of historical masonry structural systems. *Engineering Structures*, *62-63*, 118–134.

Baker, J.W. (2007). Quantitative Classification of Near-Fault Ground Motions Using Wavelet Analysis. *Bulletin of the Seismological Society of America*, *97*(5), 1486–1501.

Baker, J.W. (2008). Identification of Near-Fault Velocity Pulses and Prediction of Resulting Response Spectra. In *Proceedings of Geotechnical Earthquake*

Engineering and Soil Dynamics IV (pp. 1-10). Sacramento, California: American Society of Civil Engineers.

Boore, D.M., & Atkinson, G.M. (2008). Ground-motion prediction equations for the average horizontal component of PGA, PGV, and 5%-damped PSA at spectral periods between 0.01s and 10.0s. *Earthquake Spectra*, *24*(1), 99–138.

Bray, J.D., & Rodriguez-Marek, A. (2004). Characterization of forward-directivity ground motions in the near-fault region. *Soil Dynamics and Earthquake Engineering*, *24*, 815–28.

Campbell, K.W., & Bozorgnia, Y. (2008). NGA ground motion model for the geometric mean horizontal component of PGA, PGV, PGD, and 5% damped linear elastic response spectra for periods ranging from 0.01 to 10 s. *Earthquake Spectra*, *24*(1), 139–171.

Chiou, B.S.-J., & Youngs, R.R. (2008). An NGA model for the average horizontal component of peak ground motion and response spectra. *Earthquake Spectra*, *24*(1), 173–215.

Comité Européen de Normalisation (CEN). (2002). *EN 1991-1:2005. Eurocode 1: Actions on Structures - Part 1: General actions — Densities, self-weight, imposed loads for buildings*. Brussels: CEN.

Comité Européen de Normalisation (CEN). (2005). *EN 1998-1:2005. Eurocode 8: Design of structures for earthquake resistance - Part 1: General rules, seismic action and rules for buildings*. Brussels: CEN.

Comité Européen de Normalisation (CEN). (2005b). *EN 1998-3:2005. Eurocode 8: Design of structures for earthquake resistance - Part 3: Assessment and retrofitting of buildings*. Brussels: CEN.

Comité Européen de Normalisation (CEN). (2005c). *EN 1996-1-1: 2005. Eurocode 6: Design of Masonry Structures - Part 1-1: Rules for reinforced and unreinforced masonry*. Brussels: CEN.

Comité Européen de Normalisation (CEN). (2011). *EN 772–1:2011. Methods of test for masonry units - Part 1: Determination of compressive strength*. Brussels: CEN.

Consiglio Superiore dei Lavori Pubblici. (2009). Circolare, n. 617: Istruzioni per l'applicazione delle "Nuove norme tecniche per le costruzioni" di cui al D.M. (in Italian)

Corradi, M., Tedeschi, C., Binda, L., & Borri, A. (2008). Experimental evaluation of shear and compression strength of masonry wall before and after reinforcement: Deep repointing. *Construction and Building Materials*, *22*(4), 463–472.

Credali, L., & Ussia, G. (2011). Composite Materials Technologies in Constructions Structural Retrofitting: New Developments and Applications in Historical Buildings and Applications in Seismic Zone. In *Proceedings of the 3rd International Conference on Computational Methods in Structural Dynamics and Earthquake Engineering COMPDYN 2011* (pp. 1866-1882). Corfu, Greece: ECCOMAS.

D'Ayala, D., & Speranza, E. (2003). Definition of collapse mechanisms and seismic vulnerability of historic masonry buildings. *Earthquake Spectra*, *19*(3), 479–509.

Decreto del Presidente del Consiglio dei Ministri (D.P.C.M.). (2011). Linee guida per la valutazione e la riduzione del rischio sismico del patrimonio culturale con riferimento alle Norme tecniche per le costruzioni di cui al D.M. 14/01/2008. (in Italian)

Dizhur. D., Ingham, J., Moon, L., Griffith, M., Schultz, A., Senaldi, I., Magenes, G., Dickie, J., Lissel, S., Centeno, J., Ventura, C., Leite, J., & Lourenco, P. (2011). Performance of masonry buildings and churches in the 22 February 2011 Christchurch earthquake. *Bulletin of the New Zealand Society for Earthquake Engineering, 44*(4), 279-296.

Earthquake Planning Protection Organization (EPPO) and European Centre on Prevention and Forecasting of Earthquakes (ECPFE). (2011). Draft framework regulatory document for structural interventions to and seismic protection of monuments.

GEER-EERI-ATC. (2014). Earthquake Reconnaissance January 26th/ February 2nd 2014 Cephalonia, Greece events. GEER Association Report No. GEER-034 in collaboration with EERI and ATC, Version 1: June 6, 2014.

Greek Government Gazette (GGG). (2014). GGG 455/B/2014: Determination of minimum mandatory requirements for the preparation of surveys for the rehabilitation and the issuing of building permits for the repair and strengthening of reinforced concrete buildings, damaged by an earthquake. (in Greek)

Hellenic Organization for Standardization (ELOT). *EN 1998-1:2005. Greek National Annex to Eurocode 8: Design of structures for earthquake resistance - Part 1: General rules, seismic actions and rules for buildings*. Athens: ELOT.

Idriss, I.M. (2008). An NGA empirical model for estimating the horizontal spectral values generated by shallow crustal earthquakes. *Earthquake Spectra, 24*(1), 217–242.

Kanai, K., Tanaka, T. (1961). On Microtremos VIII. *Bulletin of Earthquake Research, 39*, 97-114.

Katsaragakis, E.S. (1987). A new tensile test for concrete. *Materials and Structures/ Materiaux et Constructions, 20*(6), 463-466.

Krawinkler, H., & Alavi, B. (1998). Development of improved design procedures for near-fault ground motions. In *Proceedings of the SMIP98 Seminar on Utilization of Strong Motion Data, California Strong Motion Instrumentation Program* (pp. 21-42). Oakland, CA; California Strong Motion Instrumentation Program.

Lagomarsino, S., Penna, A., Galasco, A., & Cattari, S. (2013). TREMURI program: An equivalent frame model for the nonlinear seismic analysis of masonry buildings. *Engineering Structures, 56*, 1787–1799.

Leucci, G., Masini, N., Persico, R., & Soldovieri, F. (2011). GPR and sonic tomography for structural restoration: The case of the cathedral of Tricarico. *Journal of Geophysics and Engineering, 8*(3), S76-S92.

Lourenço, P.B. (2005). Assessment, diagnosis and strengthening of Outeiro Church, Portugal. *Construction and Building Materials, 19*, 634-645.

Maniatakis, C.A, & Spyrakos, C.C. (2012). A new methodology to determine elastic displacement spectra in the near-fault region. *Soil Dynamics and Earthquake Engineering, 35*, 41-58.

Mavroeidis, G.P., & Papageorgiou, A.S. (2003). A Mathematical Representation of Near - Fault Ground Motions. *Bulletin of the Seismological Society of America, 93*(3), 1099 – 1131.

Mavroeidis, G.P., Dong, G., & Papageorgiou, A.S. (2004). Near-fault ground motions, and the response of elastic and inelastic single-degree-of-freedom (SDOF) systems. *Earthquake Engineering and Structural Dynamics, 33*, 1023-1049.

Mele, E., De Luca, A., & Giordano, A. (2003). Modeling and analysis of a basilica under earthquake loading. *Journal of Cultural Heritage*, *4*, 355–367.

Oliveira, D.V., & Lourenço, P.B. (2006). Experimental behaviour of three-leaf stone masonry walls. In *Proceedings of the Conference and Brokerage Event the Construction Aspects of Built Heritage Protection* (pp. 356–362). Dubrovnik, Croatia: European Construction Technology Plataform.

Pacific Earthquake Engineering Research Center (2014). Peer Strong Motion Database. Retrieved November 4, 2014 from http://ngawest2.berkeley.edu/

Palamida-Efthymiadou, T. (2007). *The Metropolis of Lemnos during the last century of Ottoman rule (1800-1912), according to the Bishopric Codes of Lemnos*. Alexandroupolis; Melissa Press. (in Greek)

Pantazopoulou, S. (2013). *State of the art report for the analysis methods for unreinforced masonry heritage structures and monuments*. European Centre on Prevention and Forecasting of Earthquakes (ECPFE) Report.

Papazachos, B.C., & Papazachou, C.B. (2003). The earthquakes of Greece. Thessaloniki: Ziti Publications.

PCM 2014.4.1. Aedes Software snc, Pisa, 2014 (www.aedes.it)

Pugi, F. (2013). Seismic analysis of masonry arch structures through the finite element model "block-joint". In *Proceeding of the 4th International Conference on Computational Methods in Structural Dynamics and Earthquake Engineering COMPDYN 2013* (pp. 2997-3014). Kos, Greece; ECCOMAS.

Royal Decree 26/19 - 2 -1959 (1959): On the seismic design of structures. (in Greek)

SEISMO - Seismic Protection of Monuments and Historical Structures. THALES Project. Operational Programme - Education and Lifelong Learning, NSRF 2007-2013. Coordinating Institution: National Technical University of Athens (NTUA).

Shahi, S.K., & Baker, J.W. (2011). An empirically calibrated framework for including the effects of near-fault directivity in Probabilistic seismic hazard analysis. *Bulletin of the Seismological Society of America*, *101*(2), 742-755.

Somerville, P.G. (1998). Development of an improved representation of near fault ground motions. In *Proceedings of the SMIP98 Seminar on Utilization of Strong Motion Data, California Strong Motion Instrumentation Program* (pp. 1-20). Oakland, CA; California Strong Motion Instrumentation Program.

Somerville, P.G., Smith, N.F., Graves, R.W., & Abrahamson, N.A. (1997). Modification of empirical strong ground motion attenuation relations to include the amplitude and duration effects of rupture directivity. *Seismological Research Letters*, *68*, 199-205.

Spyrakos, C.C. (1995). *Finite Element Modeling in Engineering Practice*. Pittsburg, PA, USA: Algor Publishing Division.

Spyrakos, C.C. (2004). Strengthening of structures for seismic loads. Athens: Technical Chamber of Greece. (in Greek)

Spyrakos, C.C., & Raftoyiannis, J. (1997). *Linear and Nonlinear Finite Element Analysis*. Pittsburg, PA, USA: Algor Publishing Division.

Spyrakos, C.C., & Maniatakis, C.A. (2006). Retrofitting of a Historic Masonry Building. In *Proceedings of the 10th National and 4th International scientific meeting on Planning, Design, Construction and Renewal in the construction industry iNDiS 2006* (pp. 535-544). Novi Sad: Faculty of Technical Sciences, Institute for Civil Engineering.

Spyrakos, C.C., Maniatakis, C.A., & Taflambas, J. (2008). Evaluation of near source seismic records based on damage potential parameters: Case study: Greece. *Soil Dynamics and Earthquake Engineering, 28*, 738-753.

Spyrakos, C.C., Kiriakopoulos, P.D., & Smyrou, E. (2011). Seismic Strengthening of the Historic Church of Sts Helen and Constantine in Piraeus. In *Proceedings of the 3rd International Conference on Computational Methods in Structural Dynamics and Earthquake Engineering COMPDYN 2011*. Corfu, Greece; ECCOMAS.

Spyrakos, C.C., Maniatakis, C.A., Smyrou, E., & Psycharis, I.N. (2012). FRP Strengthened Brick-Infilled RC Frames: An Approach for their Proper Consideration in Design. *The Open Construction and Building Technology Journal*, *6*(Suppl 1-M19), 306-324.

Spyrakos, C.C., Francioso, A., Kiriakopoulos, P.D., & Papoutsellis, S. (2013). Seismic evaluation of the historic church of St. Nicholas in Piraeus before and after interventions. In *Proceeding of the 4th International Conference on Computational Methods in Structural Dynamics and Earthquake Engineering COMPDYN 2013* (pp. 3015-3029). Kos, Greece; ECCOMAS.

Spyrakos, C.C., Touliatos, P., Patsilivas, D., Pelekis, G., Xampesis, A., & Maniatakis, C.A. (2013b). Seismic analysis and retrofit of a historic masonry building. In Syngellakis, S. (Ed.), *Retrofitting of Heritage Structures - Design and evaluation of strengthening techniques* (pp. 65-74). Southampton, UK: Wessex Institute of Technology Press.

Spyrakos, C.C., Maniatakis, C.A., & Taflambas J. (2015). Critical evaluation of near field seismic records in Greece. In Syngellakis, S. (Ed.), *Earthquake Ground Motion - Input Definition for Aseismic Design* (pp. 1-10). Southampton, UK: Wessex Institute of Technology Press.

Stewart, J.P., Chiou, S.J., Bray, J.D., Graves, R.W., Somerville, P.G., & Abrahamson, N.A. (2001). Ground Motion Evaluation Procedures for Performance-Based Design. USA California, Berkeley: University of California, Berkeley, Pacific Earthquake Engineering Research Center, PEER-2001/09; 2001.

Taflampas, I.M., Spyrakos, C.C., Maniatakis, C.A. (2008). A new definition of strong motion duration and related parameters affecting the response of medium-long period structures. In *Proceedings of the 14th World Conference in Earthquake Engineering* (No. 03-01-0057). Beijing, China: International Association for Earthquake Engineering.

Taflampas, I.M., Spyrakos, C.C., Koutromanos, I.A. (2009). A new definition of strong motion duration and related parameters affecting the response of medium-long period structures. *Soil Dynamics and Earthquake Engineering, 29*, 752–763.

Tassios, T.P., Chronopoulos, M.P. (1986). *Pathological Causes and Mechanics of Damage for Masonry*. Athens: National Technical University of Athens. (in Greek)

Tassios, T.P. (1988). *Meccanica delle murature*. Napoli: Liguori Editore. (in italian)

Tassios, T.P., Vachliotis, C., & Spanos, C. (1990). In-Situ Strength Measurements of Masonry Mortars. In *Proceedings of the International Technical Conference on Structural Conservation of Stone Masonry* (pp. 53-61). Athens: ICCROM.

Tassios, T.P. (2010). Seismic Engineering of Monuments. In Garevski, M., & Ansal. A. (Ed.), *Earthquake engineering in Europe* (pp. 1-42). Springer Netherlands.

Titman, D.J. (2001). Applications of thermography in non-destructive testing of structures. *NDT & E International*, *34*(2), 149-154.

Tomaževič, M. (1999). *Earthquake-Resistant Design of Masonry Buildings*. London: Imperial College Press.

Tourptsoglou-Stefanidou, V. (1986). *Travel and Geography documents for Lemnos (15th-20th c.)*. Thessaloniki: Aristotle University of Thessaloniki. (in Greek)

Tsapanos, T.M., & Burton, P.W. (1991). Seismic hazard evaluation for specific seismic regions of the world. *Tectonophysics*, *194*, 153–169.

U.S. Geological Survey – USGS (2014). *M6.9 - 22km SSW of Kamariotissa, Greece (BETA)*. Retrieved November 4, 2014 from http://comcat.cr.usgs.gov/earthquakes/eventpage/usb000r2hc#summary

Valluzzi, M.R., Porto, F.D., & Modena, C. (2004). Behavior and modeling of strengthened three-leaf stone masonry walls. *Materials and Structures/ Materiaux et Constructions*, *37*, 184-192.

Vintzileou, E., & Miltiadou-Fezans, A. (2008). Mechanical properties of three-leaf stone masonry grouted with ternary or hydraulic lime-based grouts. *Engineering Structures*, *30*(8), 2265–2276.

LIST OF TABLES

Table 1. Results of SPT test

Depth (m)	SPT	N_{SPT}
0.50 ~ 0.64	50/14	>50
3.00 ~ 3.45	7-13-25	38
5.50 ~ 5.78	24-50/13	>50
10.00 ~10.35	30-33-50/35	>50

Table 2. Results of Ambient Vibration measurements

Direction	Eigenfrequency - Hz (Eigenperiod - sec)
WE	4.39 (0.22)
NS	5.86 (0.17)

Table 3: Mechanical characteristics of masonry

	Mechanical property		Initial state	After interventions
Stones	Compressive strength	f_{bc} (N/mm^2)	45.82	45.82
Mortar	Compressive strength	f_{mc} (N/mm^2)	1	1.91
Bricks	Compressive strength	f_b (N/mm^2)	2.15	2.15
	Modulus of Elasticity	E_b (N/mm^2)	2150	2150
Masonry	Compressive strength	f_c (N/mm^2)	4.01	4.47
	Tensile strength	f_t (N/mm^2)	0.40	0.45
	Modulus of Elasticity	E (N/mm^2)	4013	4470
	Specific weight	W (kN/m^3)	26	26

Table 4. Modal periods and related spectral accelerations

Status	Direction	First period	Spectral acceleration (g) EC-8 (q=1.5)	GC-59 (q=1.5)	NF-1 (q=1.5)	NF-5 (q=1.5)
Initial state	x-x (WE)	0.204	0.48	0.24	0.574	0.388
	y-y (NS)	0.172	0.48	0.24	0.572	0.381
After interventions	x-x (WE)	0.185	0.48	0.24	0.573	0.383
	y-y (NS)	0.157	0.48	0.24	0.572	0.376

Table 5. Results of kinematic limit analyses.

Collapse mechanism	α_0	α_0^* (g)	EC8		NF-1		NF-5	
			α_{Rig}^* (g)	α_{Def}^* (g)	α_{Rig}^* (g)	α_{Def}^* (g)	α_{Rig}^* (g)	α_{Def}^* (g)
North façade (mezzanine wall)	0.243	0.185	0.173	0.203	0.233	0.242	0.147	0.163
Central apse	0.162	0.142	0.173	-	0.233	-	0.147	-

FIGURE CAPTIONS

Figure 1: Exact location of Lemnos Island in the North-East Aegean Sea. With dashed line the traces of North Anatolian fault are shown

Figure 2. Plan view of the St. Demetrius Church

Figure 3. Geotechnical investigation: (a); soil profile; (b) amplified spectra at soil surface

Figure 4. Major cracks in the masonry structure: (a) frontage (west façade); (b) south façade; (c) east façade; (d) north façade

Figure 5. Signs of corrosion: (a) external tie-rods at the west façade; (b) fully corroded steel plate supporting a cross-vault

Figure 6. Characterization of mortar: (a) optical microscopy; (b) sample of mortar including natural limestone aggregates with dimensions ≥2mm; (c) X-ray analysis results

Figure 7. Results of Infrared Thermography method at selected locations: (a) moisture detection near a closed window; (b) humidity detection at the base of a cross-vault

Figure 8. Endoscopy at the external wall next to the southern main entrance in the west façade: (a) drilling of the inspection hole; (b) interior view

Figure 9. Ambient Vibration testing at indicative positions: (a) ground floor beneath the central dome; (b) roof of the mezzanine

Figure 10. Ambient vibration testing in the West-East direction: (a) Placement of instruments; (b) Transfer function

Figure 11. Comparison of different spectra applied in the analyses

Figure 12. General views of the finite element model: (a) three dimensional view; (b) sectional view along the west-east direction

Figure 13. Eigenvalue analysis of the initial structure: (a) 1^{st} mode of vibration; (b) 2^{nd} mode of vibration; (c) 3^{rd} mode of vibration

Figure 14. Validation of the finite element model: (a) position of tensile failure at the north façade; (b) confirmation of crack existence in the same place

Figure 15. West façade - Distribution of maximum stresses in the original model without interventions for the G+0.5Q+Ex+0.3Ey combination: (a) Eurocode 8 spectrum; (b) 1959-Greek Seismic Code spectrum; (c) Near-fault spectrum with R=1 km

Figure 16. East façade - Distribution of maximum stresses in the original model without interventions for the G+0.5Q+Ex+0.3Ey combination: (a) Eurocode 8 spectrum; (b) 1959-Greek Seismic Code spectrum; (c) Near-fault spectrum with R=1 km

Figure 17. South façade - Distribution of maximum stresses in the original model without interventions for the G+0.5Q+Ex+0.3Ey combination: (a) Eurocode 8 spectrum; (b) 1959-Greek Seismic Code spectrum; (c) Near-fault spectrum with R=1 km

Figure 18. North internal façade - Distribution of maximum stresses in the original model without interventions for the G+0.5Q+Ex+0.3Ey combination: (a) Eurocode 8 spectrum; (b) 1959-Greek Seismic Code spectrum; (c) Near-fault spectrum with R=1 km

Figure 19. Failure according to capacity exceedance. Yellow color for 0,90≤α≤1,1; Red color for α>1,1; Magenta for tensile failure. (a) In-plane flexure; (b) Shear; (c) Out-of-plane flexure. (I) West façade; (II) South - north façade

Figure 20. Selection of different local collapse mechanisms: (a) overturning of a structural part in the north façade; (b) overturning of the central apse in the east façade

Figure 21. Strengthening with CFRPs: (a) west façade; (b) south & north façade; (c) roof; (d) cross-vault

Figure 22. West façade - Distribution of maximum stresses in the strengthened model for the G+0.5Q+Ex+0.3Ey combination: (a) Eurocode 8 spectrum; (b) 1959-Greek Seismic Code spectrum; (c) Near-fault spectrum with R=1 km

Figure 23. East façade - Distribution of maximum stresses in the strengthened model for the G+0.5Q+Ex+0.3Ey combination: (a) Eurocode 8 spectrum; (b) 1959-Greek Seismic Code spectrum; (c) Near-fault spectrum with R=1 km

Figure 24. South façade - Distribution of maximum stresses in the strengthened model for the G+0.5Q+Ex+0.3Ey combination: (a) Eurocode 8 spectrum; (b) 1959-Greek Seismic Code spectrum; (c) Near-fault spectrum with R=1 km

Figure 25. North internal façade - Distribution of maximum stresses in the strengthened model for the G+0.5Q+Ex+0.3Ey combination: (a) Eurocode 8 spectrum; (b) 1959-Greek Seismic Code spectrum; (c) Near-fault spectrum with R=1 km

Figure 1: Exact location of Lemnos Island in the North-East Aegean Sea. With dashed line the traces of North Anatolian fault are shown

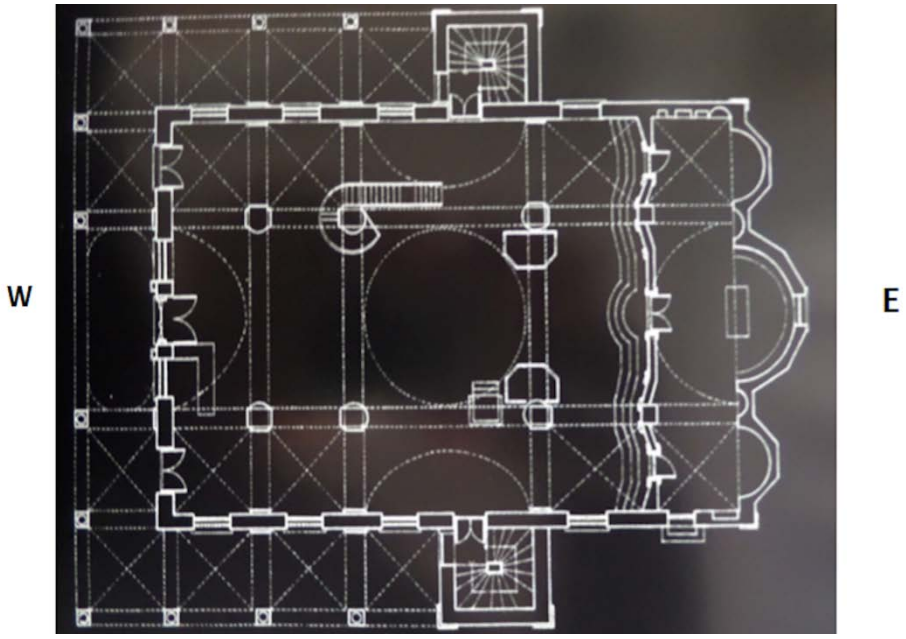

Figure 2. Plan view of the St. Demetrius Church

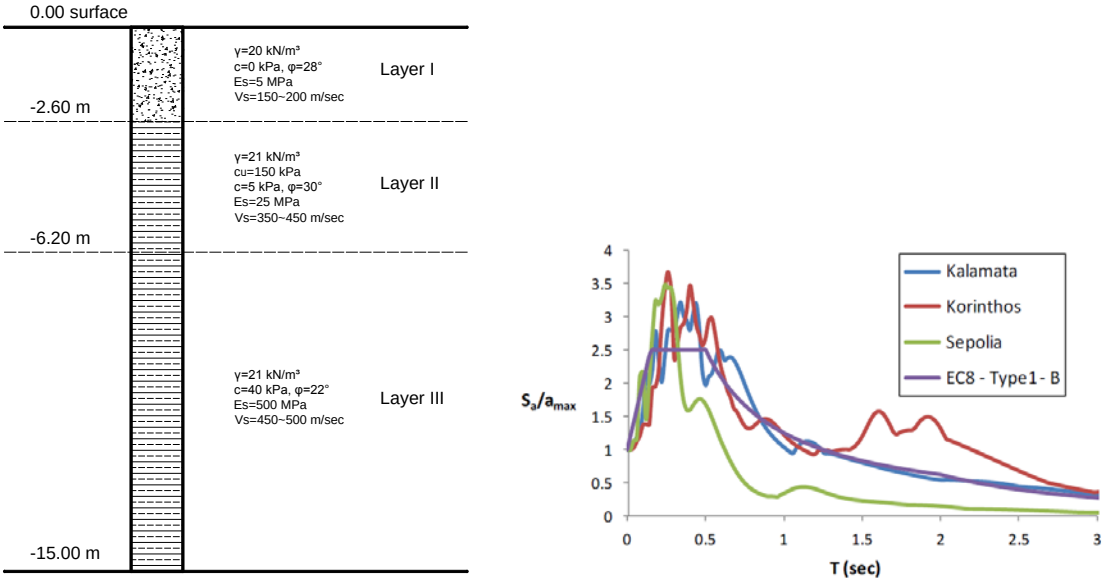

(a) (b)

Figure 3. Geotechnical investigation: (a); soil profile; (b) amplified spectra at soil surface

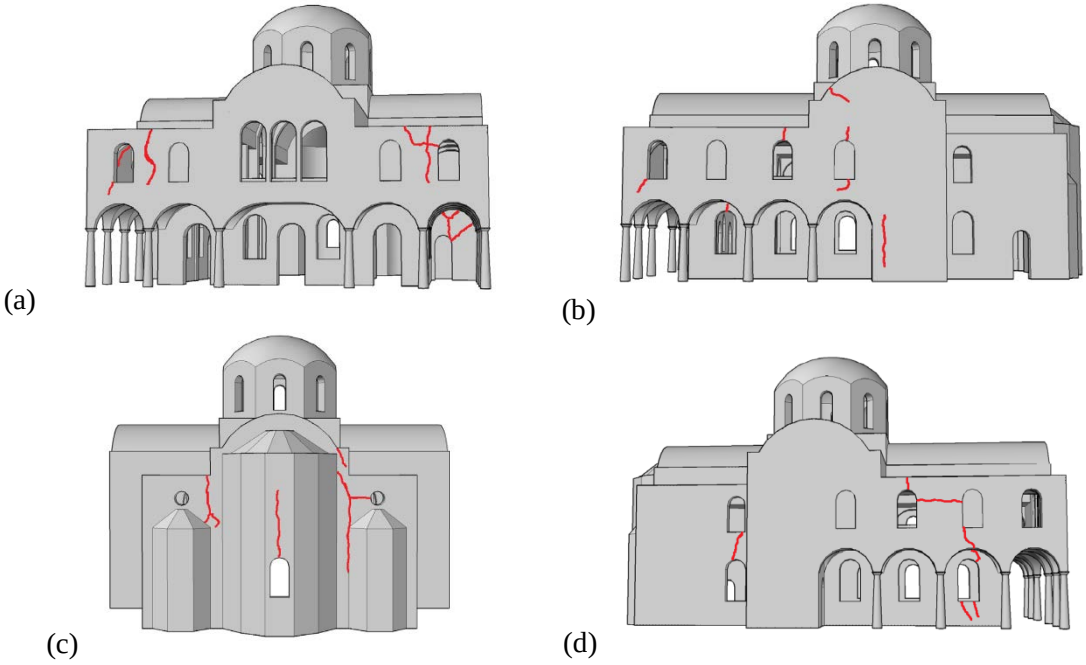

Figure 4. Major cracks in the masonry structure: (a) frontage (west façade); (b) south façade; (c) east façade; (d) north façade

(a)

(b)

Figure 5. Signs of corrosion: (a) external tie-rods at the west façade; (b) fully corroded steel plate supporting a cross-vault

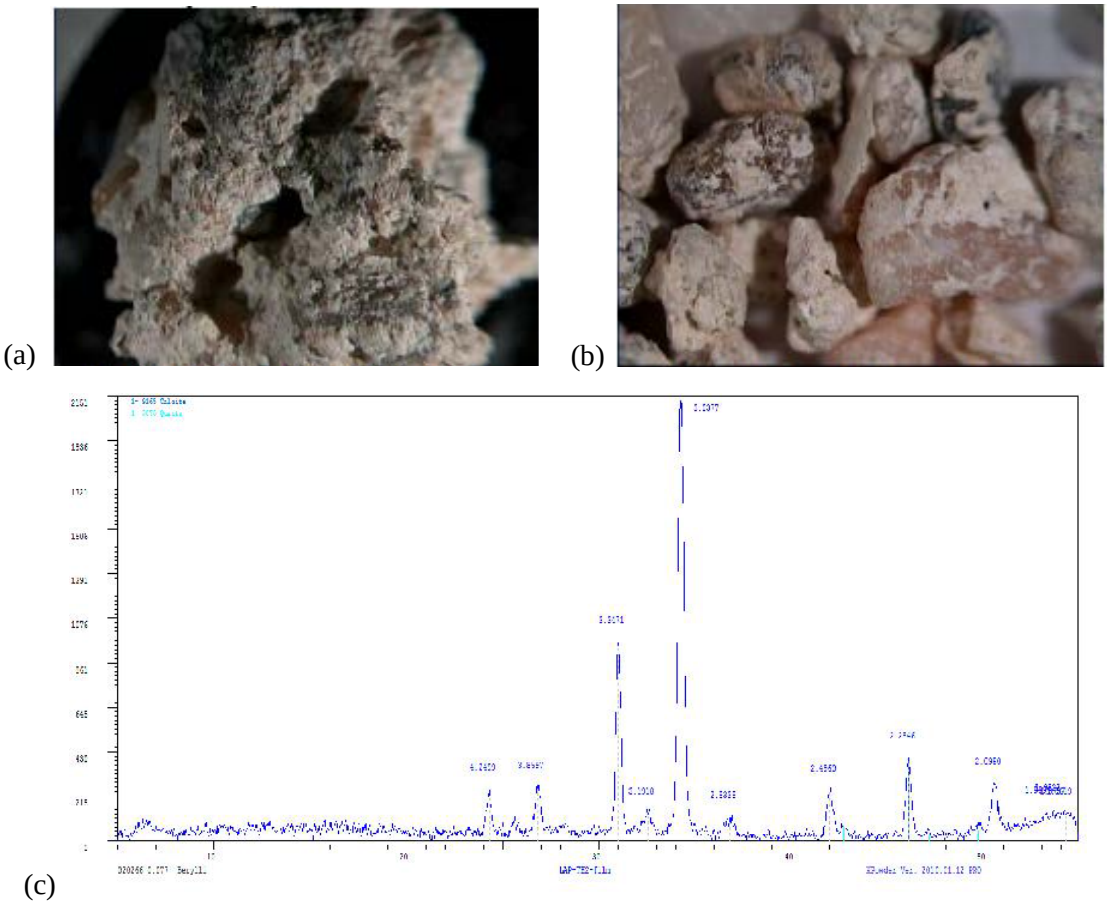

Figure 6. Characterization of mortar: (a) optical microscopy; (b) sample of mortar including natural limestone aggregates with dimensions ≥2mm; (c) X-ray analysis results

(a) (b)

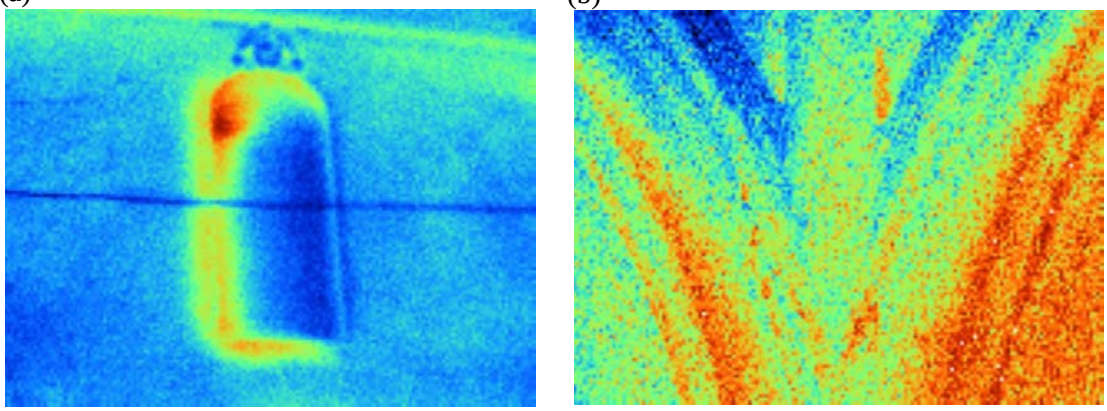

Figure 7. Results of Infrared Thermography method at selected locations: (a) moisture detection near a closed window; (b) humidity detection at the base of a cross-vault

(a) (b)

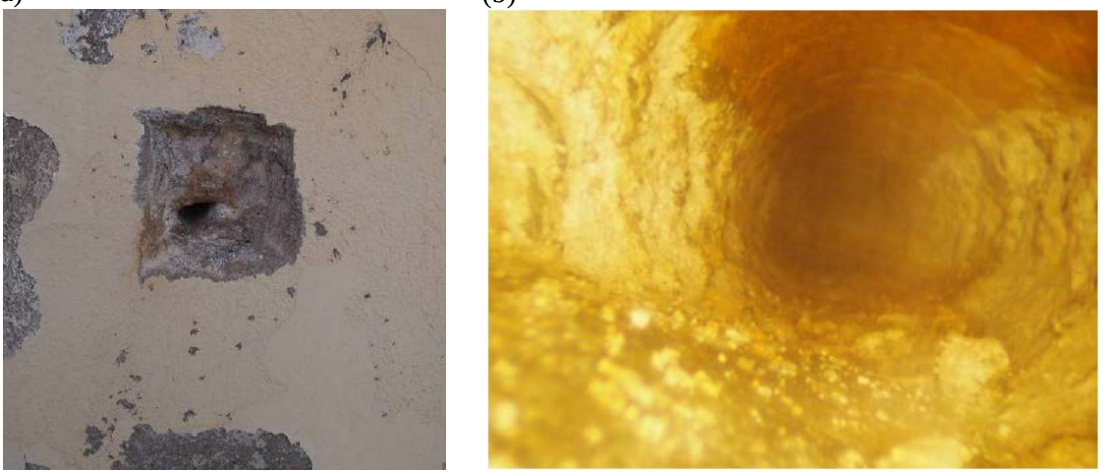

Figure 8. Endoscopy at the external wall next to the southern main entrance in the west façade: (a) drilling of the inspection hole; (b) interior view

(a) (b)

Figure 9. Ambient Vibration testing at indicative positions: (a) ground floor beneath the central dome; (b) roof of the mezzanine

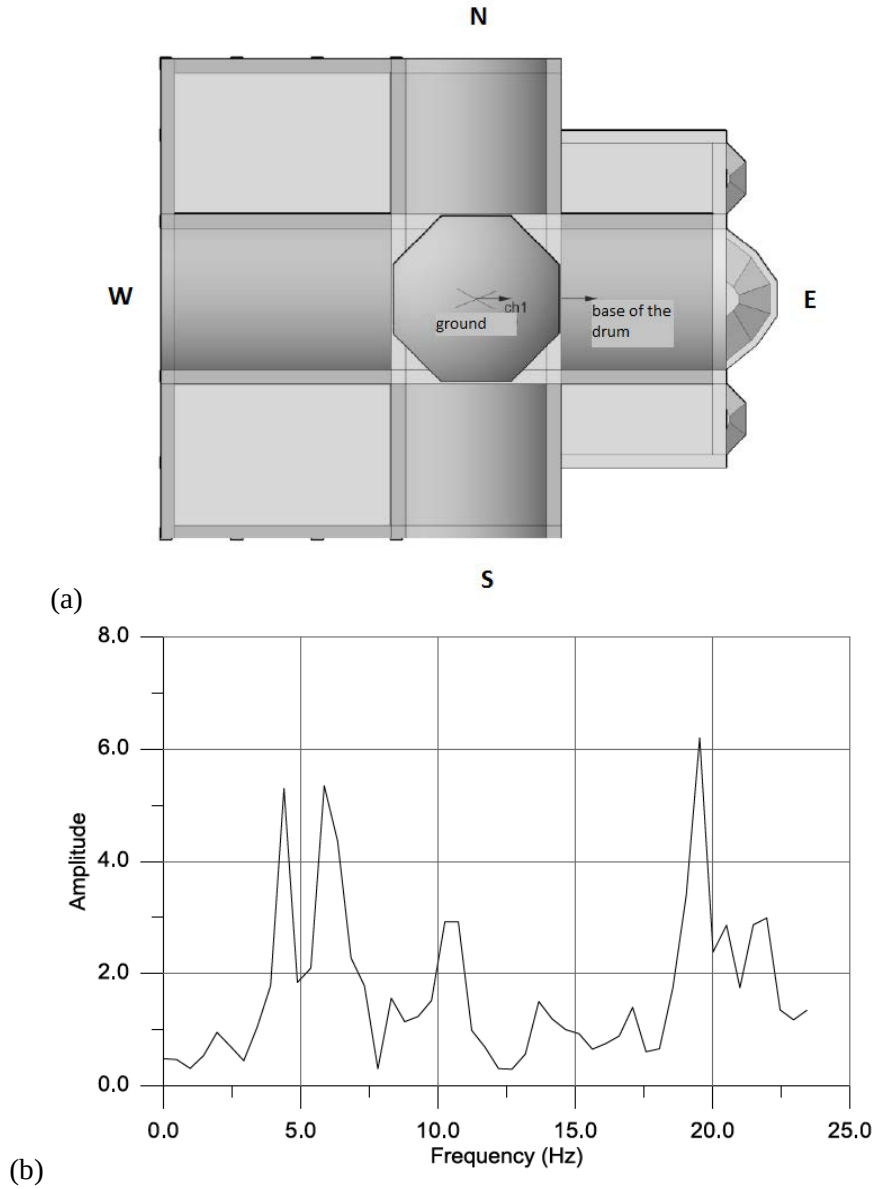

Figure 10. Ambient vibration testing in the West-East direction: (a) Placement of instruments; (b) Transfer function

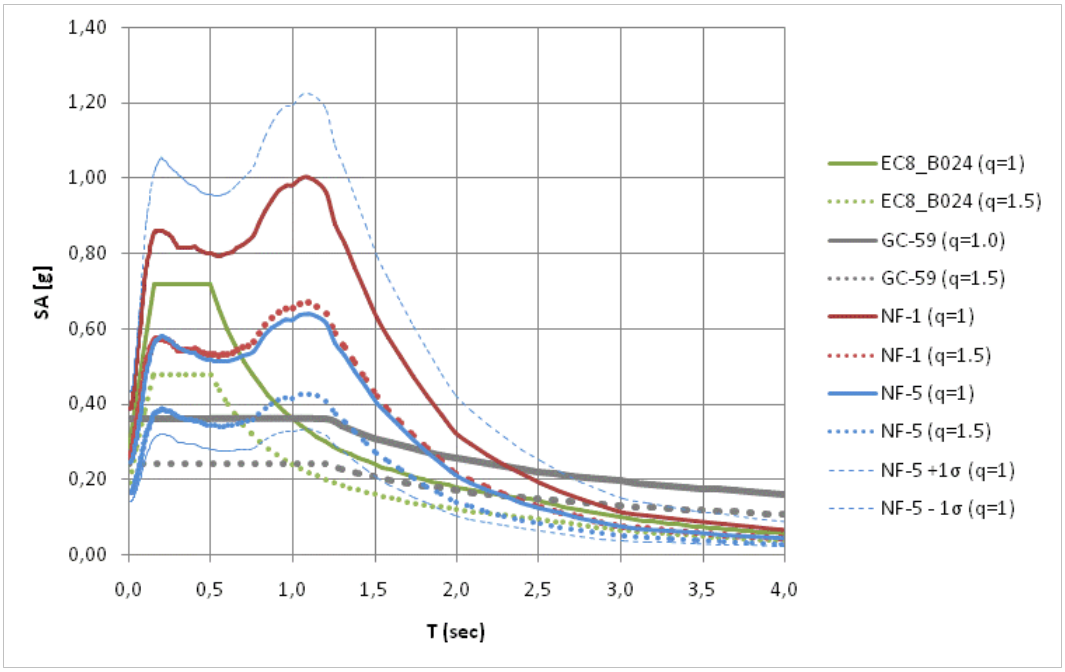

Figure 11. Comparison of different spectra applied in the analyses

(a) (b)

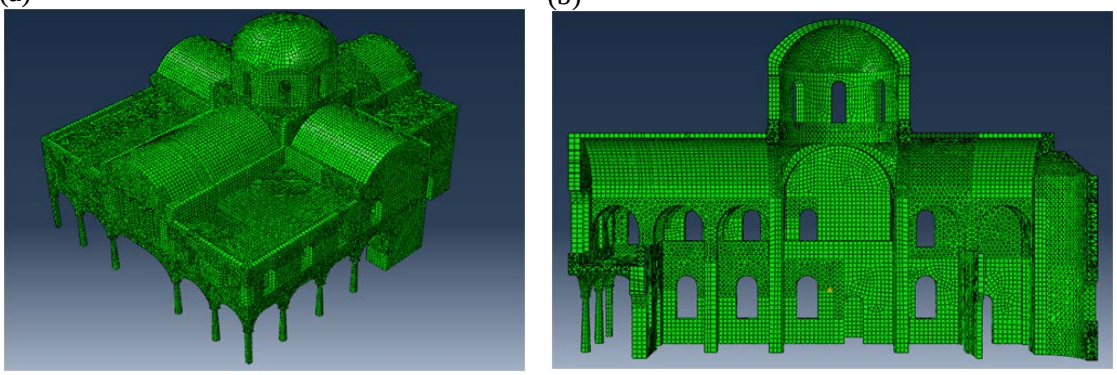

Figure 12. General views of the finite element model: (a) three dimensional view; (b) sectional view along the west-east direction

(a) (b)

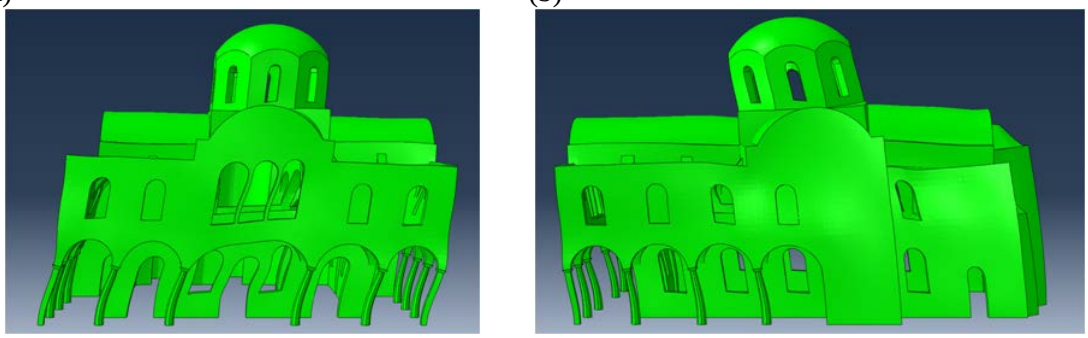

(c)

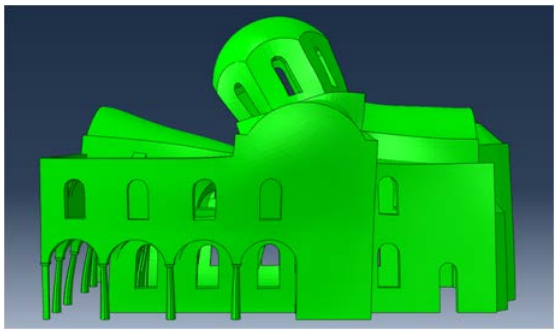

Figure 13. Eigenvalue analysis of the initial structure: (a) 1st mode of vibration; (b) 2nd mode of vibration; (c) 3rd mode of vibration.

(a) (b)

Figure 14. Validation of the finite element model: (a) position of tensile failure at the north façade; (b) confirmation of crack existence in the same place

(a)

(b)

(c)

Figure 15. West façade - Distribution of maximum stresses in the original model without interventions for the G+0.5Q+Ex+0.3Ey combination: (a) Eurocode 8 spectrum; (b) 1959-Greek Seismic Code spectrum; (c) Near-fault spectrum with R=1 km

(a)

(b)

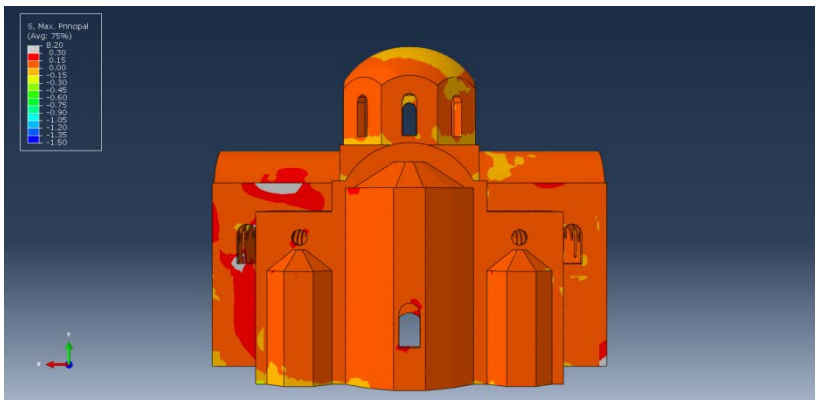

(c)

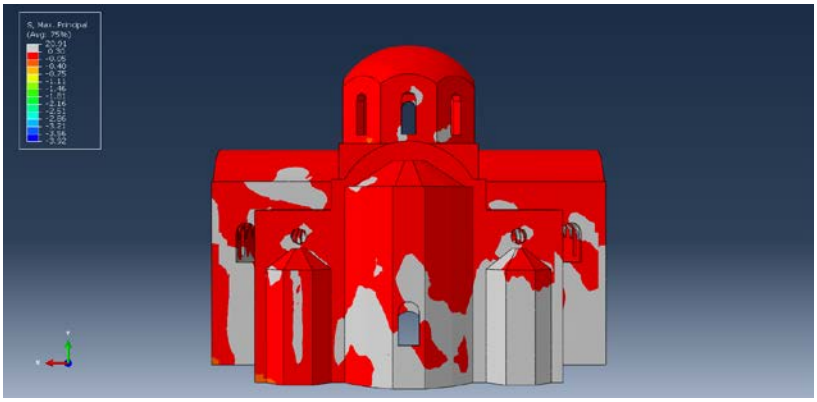

Figure 16. East façade - Distribution of maximum stresses in the original model without interventions for the G+0.5Q+Ex+0.3Ey combination: (a) Eurocode 8 spectrum; (b) 1959-Greek Seismic Code spectrum; (c) Near-fault spectrum with R=1 km

(a)

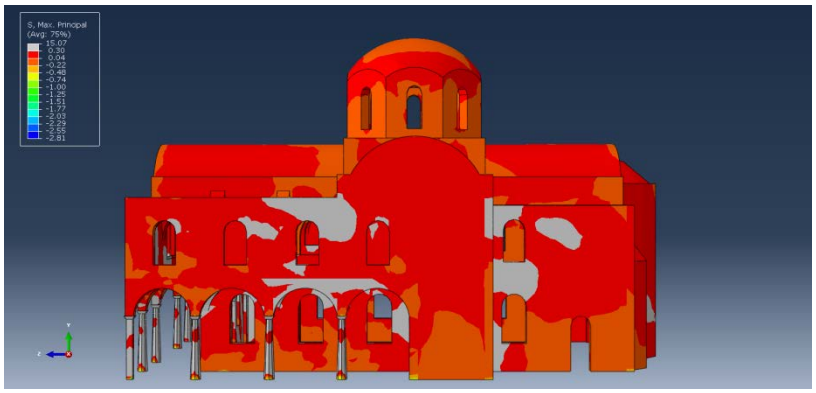

(b)

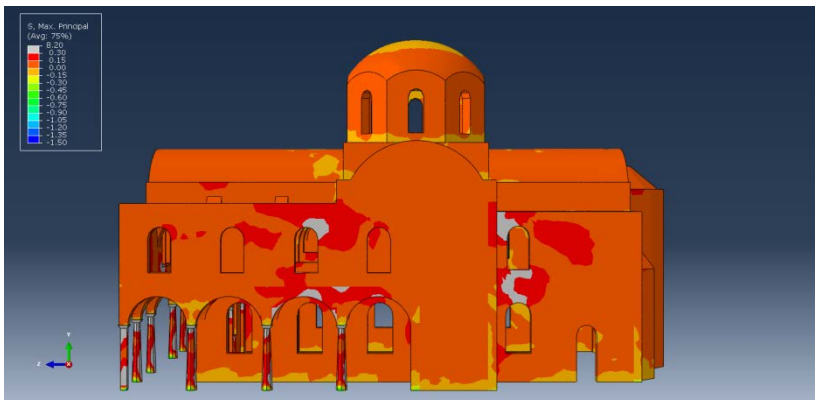

(c)

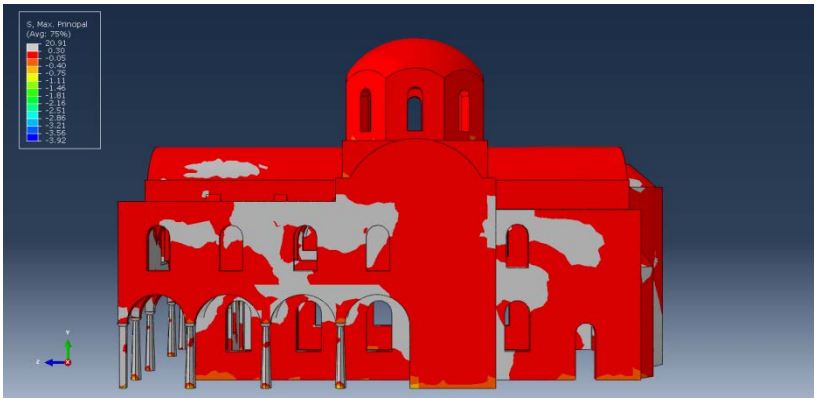

Figure 17. South façade - Distribution of maximum stresses in the original model without interventions for the G+0.5Q+Ex+0.3Ey combination: (a) Eurocode 8 spectrum; (b) 1959-Greek Seismic Code spectrum; (c) Near-fault spectrum with R=1 km

(a)

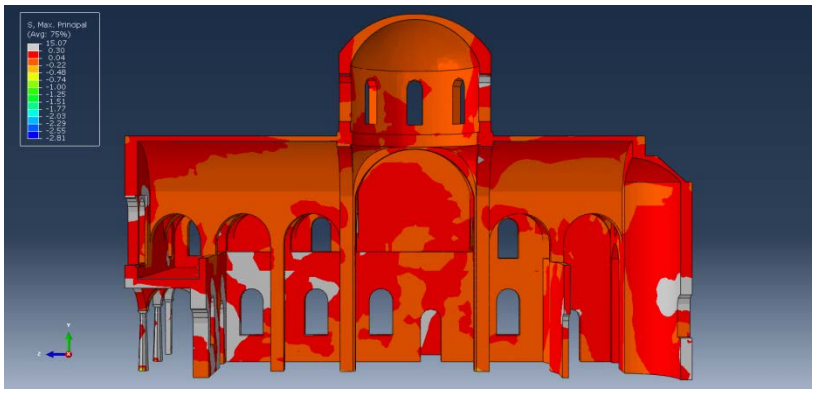

(b)

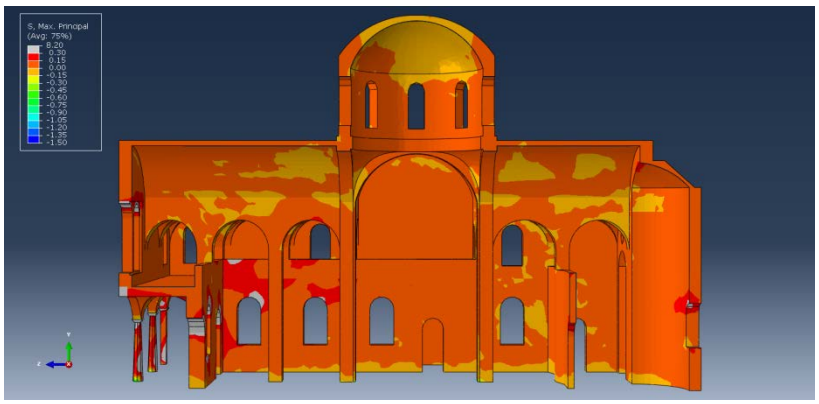

(c)

Figure 18. North internal façade - Distribution of maximum stresses in the original model without interventions for the G+0.5Q+Ex+0.3Ey combination: (a) Eurocode 8 spectrum; (b) 1959-Greek Seismic Code spectrum; (c) Near-fault spectrum with R=1 km

(I) (II)

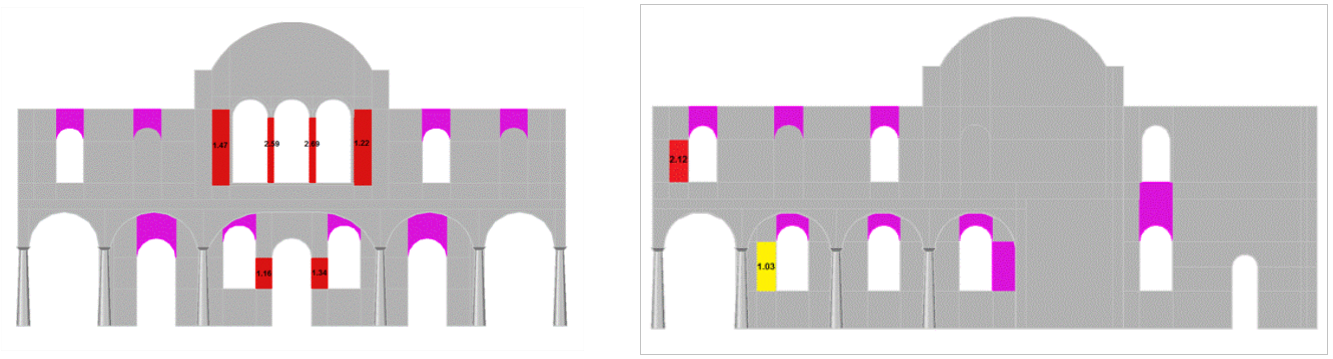

(a)

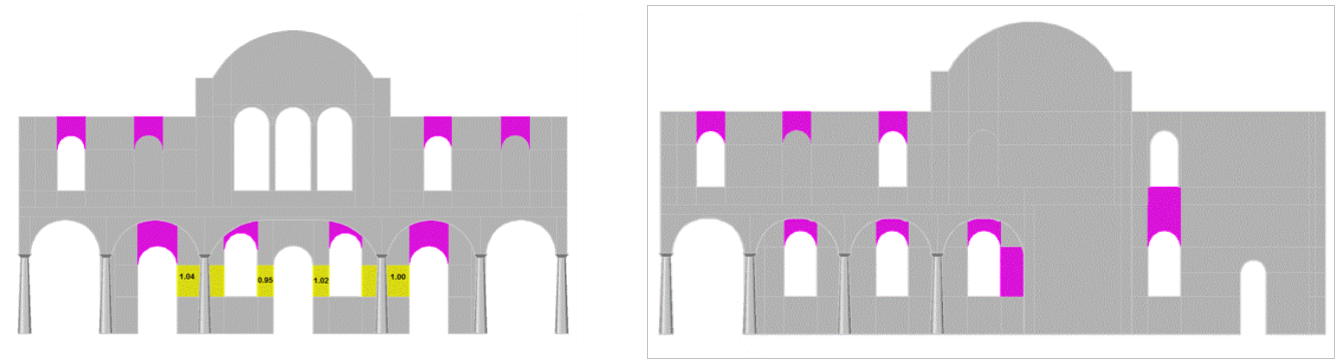

(b)

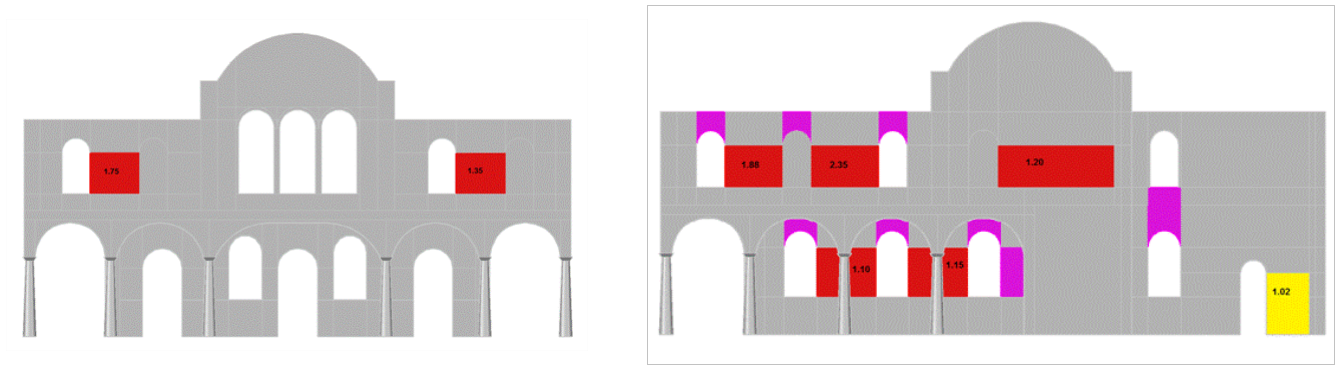

(c)

Figure 19. Failure according to capacity exceedance. Yellow color for 0,90≤α≤1,1; Red color for α>1,1; Magenta for tensile failure. (a) In-plane flexure; (b) Shear; (c) Out-of-plane flexure. (I) West façade; (II) South - north façade

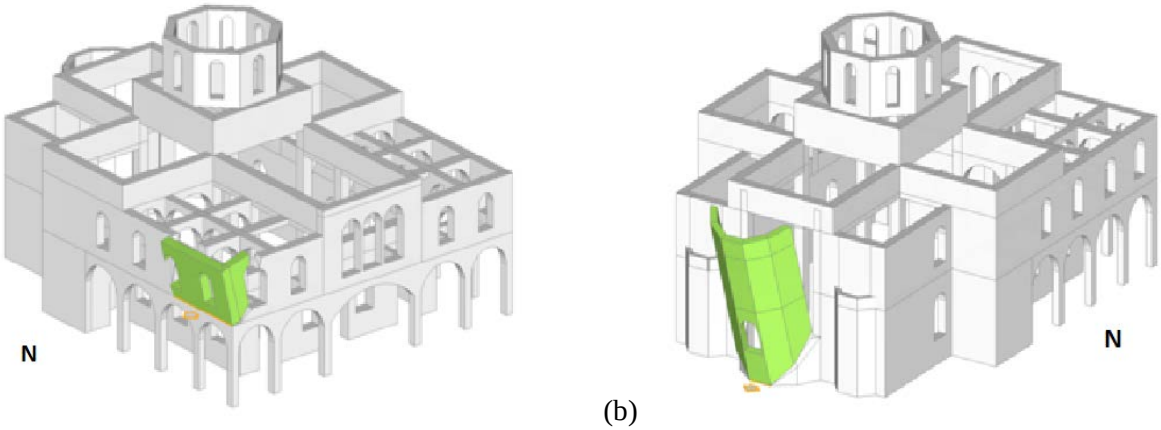

(a) (b)

Figure 20. Selection of different local collapse mechanisms: (a) overturning of a structural part in the north façade; (b) overturning of the central apse in the east façade

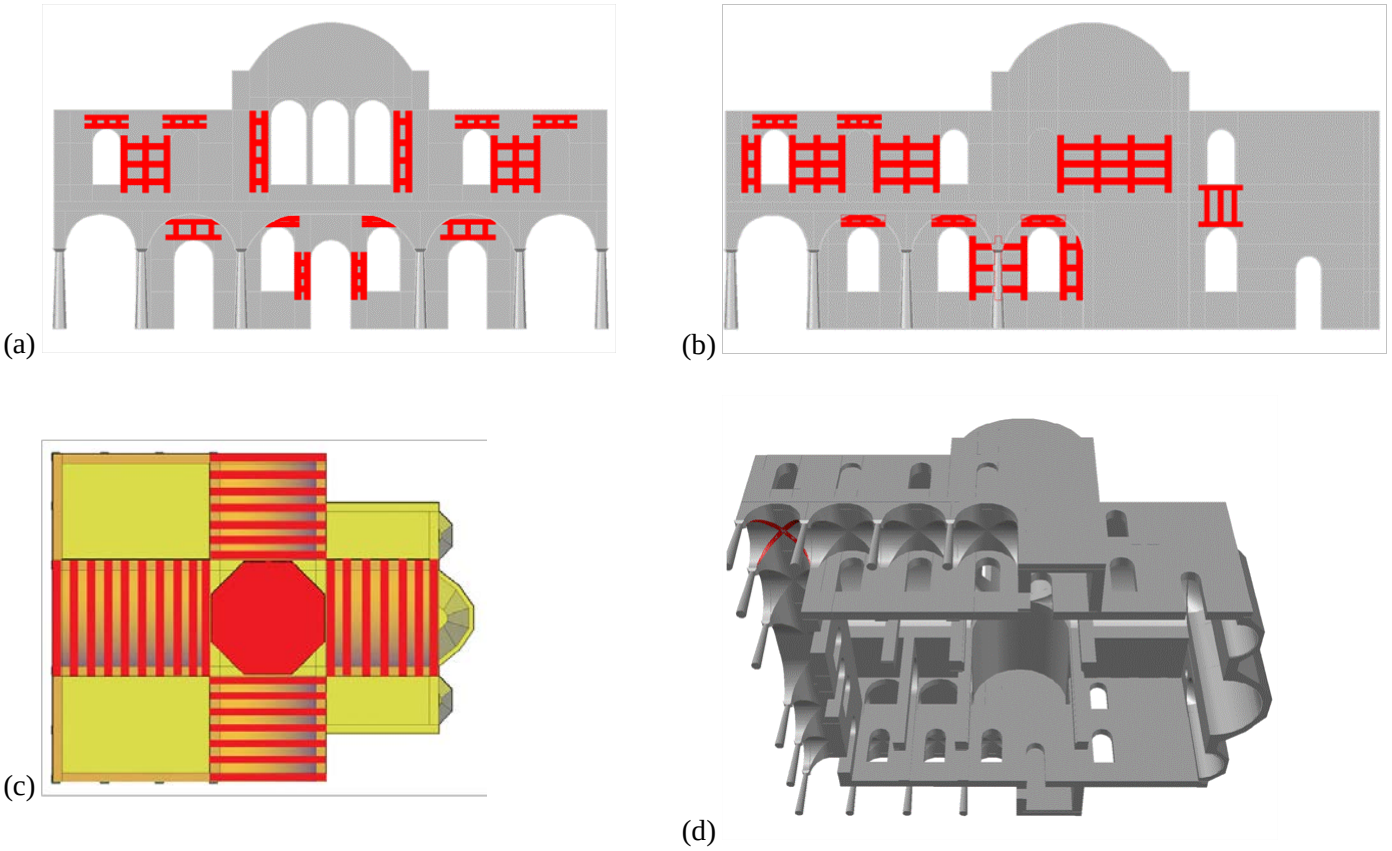

Figure 21. Strengthening with CFRPs: (a) west façade; (b) south & north façade; (c) roof; (d) cross-vault

(a)

(b)

(c)

Figure 22. West façade - Distribution of maximum stresses in the strengthened model for the G+0.5Q+Ex+0.3Ey combination: (a) Eurocode 8 spectrum; (b) 1959-Greek Seismic Code spectrum; (c) Near-fault spectrum with R=1 km

(a)

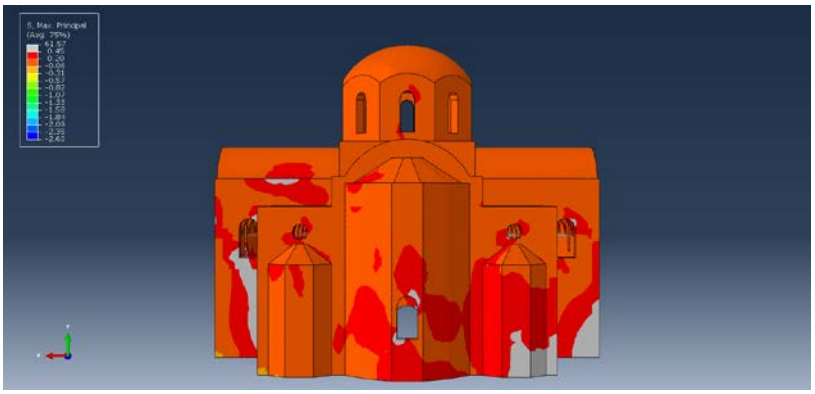

(b)

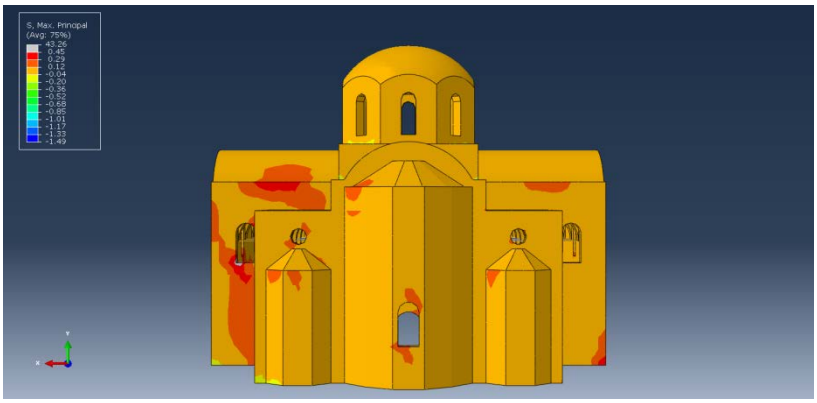

(c)

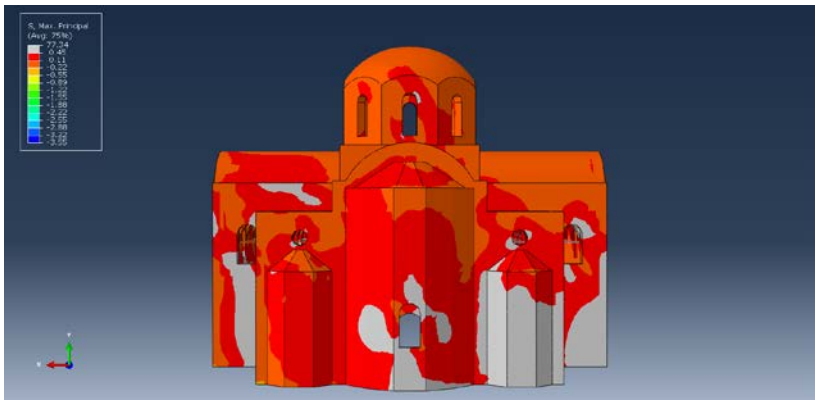

Figure 23. East façade - Distribution of maximum stresses in the strengthened model for the G+0.5Q+Ex+0.3Ey combination: (a) Eurocode 8 spectrum; (b) 1959-Greek Seismic Code spectrum; (c) Near-fault spectrum with R=1 km

(a)

(b)

(c)

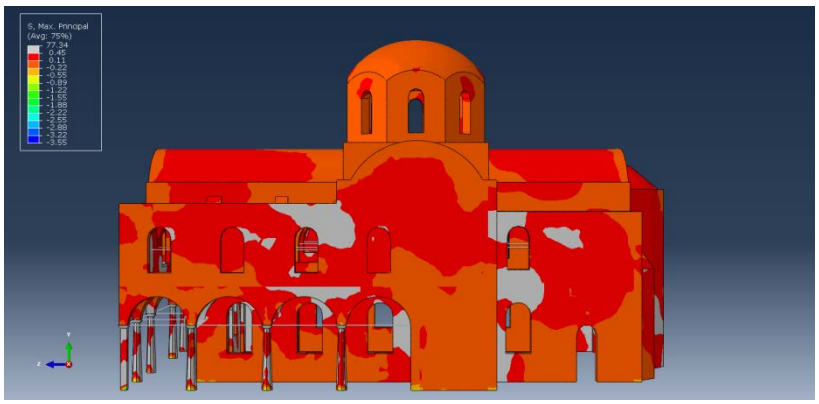

Figure 24. South façade - Distribution of maximum stresses in the strengthened model for the G+0.5Q+Ex+0.3Ey combination: (a) Eurocode 8 spectrum; (b) 1959-Greek Seismic Code spectrum; (c) Near-fault spectrum with R=1 km

(a)

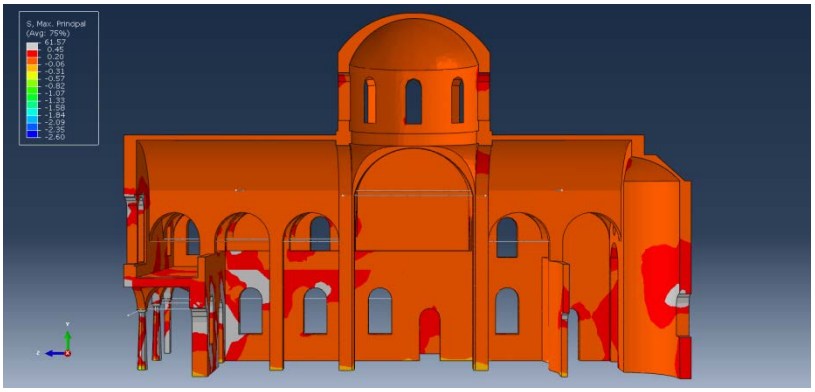

(b)

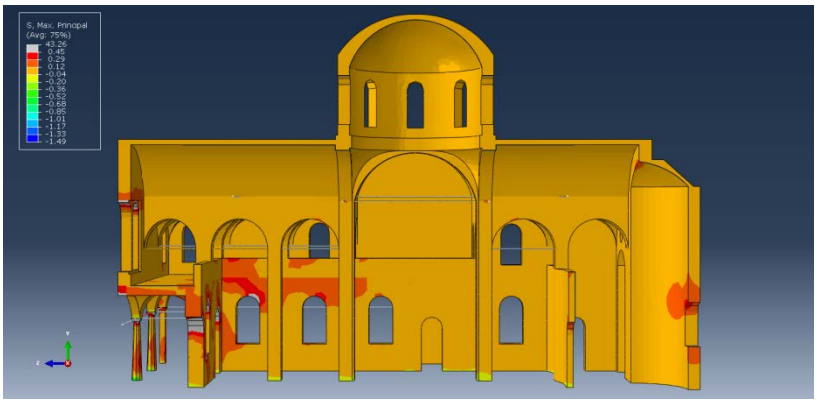

(c)

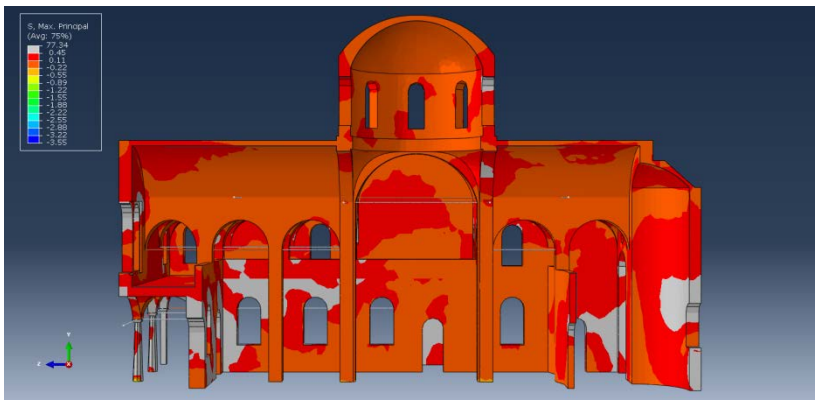

Figure 25. North internal façade - Distribution of maximum stresses in the strengthened model for the G+0.5Q+Ex+0.3Ey combination: (a) Eurocode 8 spectrum; (b) 1959-Greek Seismic Code spectrum; (c) Near-fault spectrum with R=1 km